A Bifurcation Analysis of Size Structured Phyto-Zooplankton Models.

June 20, 2025

Rolf Scheffers

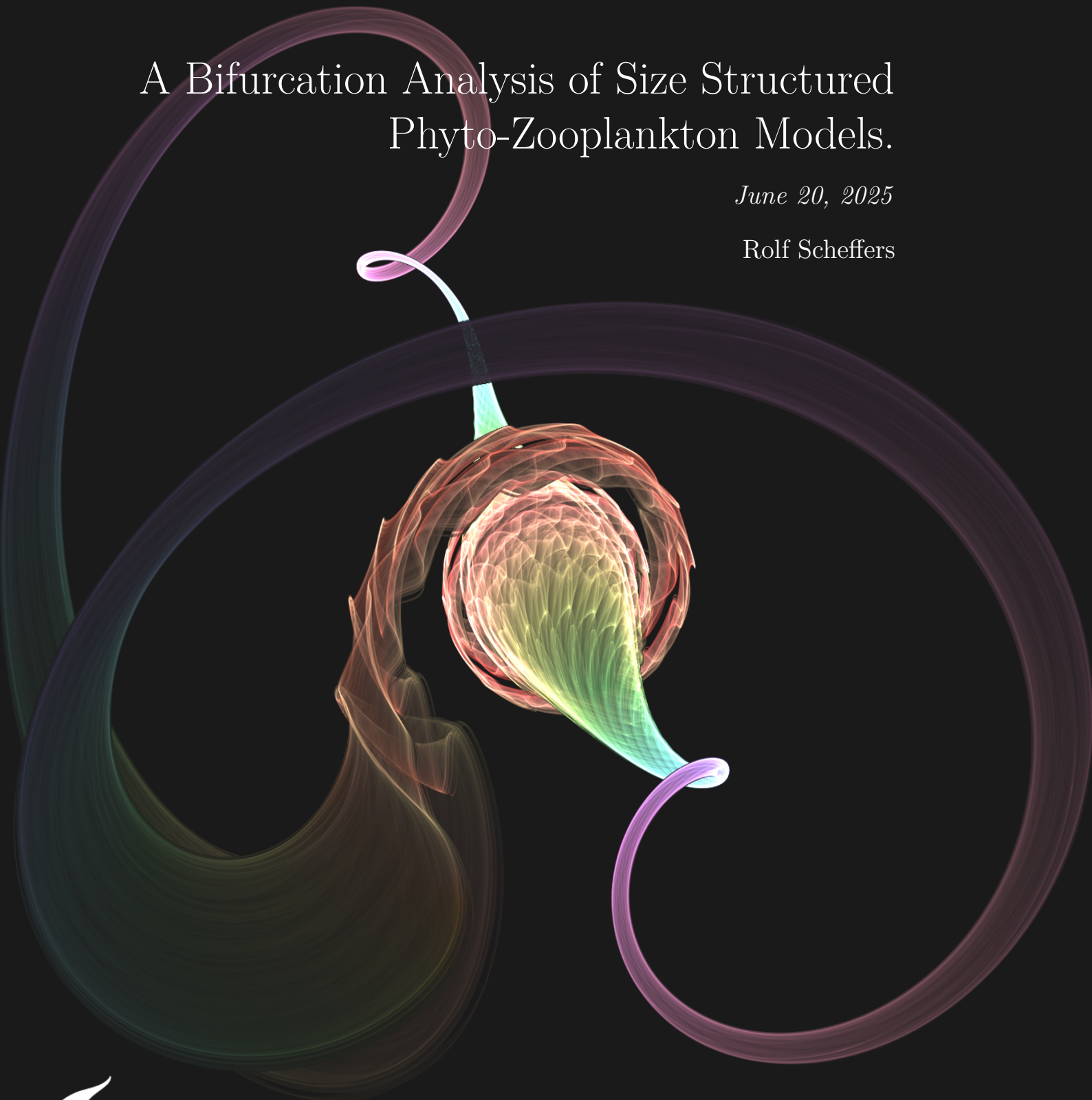

TU Delft

A Bifurcation Analysis of Size Structured Phyto-Zooplankton Models.

THESIS

submitted in partial fulfillment of the
requirements for the degree of

MASTER OF SCIENCE

in

APPLIED MATHEMATICS

by

Rolf Scheffers
born in Rotterdam, the Netherlands

Mathematical Physics Research Group
Department of Applied Mathematics
Faculty EEMCS, Delft University of Technology
Delft, the Netherlands
www.ewi.tudelft.nl

A Bifurcation Analysis of Size Structured Phyto-Zooplankton Models.

Author: Rolf Scheffers
Student id: 4855140

Abstract

Modeling plankton communities has been an import topic in mathematical biology for quite some time. Previous research mostly comes in two flavors. On one hand we have large global models, which try and recreate measured data, but often lose track of what are the root causes of phenomena. On the other hand we have smaller models, where the (mathematical) reasoning behind phenomena are tried to be understood, but they lose some of their applicability. We try to bridge the gap between these two, by exploring how far results after simplification carry over to a more general case. We do this by investigating a size structured plankton model as proposed by (Poulin & Franks, 2010). We first simplify the interaction between phyto- and zooplankton, for which we are able to find analytical stationary solutions. Using numerical methods we are able to show stable stationary and limit cycle behavior. Furthermore we are able to show how much diversity remains, and how this is linked to the analytical solutions. Then we are able to show that these structures remain in place after allowing more complex interactions, and identify how far this remains true. Using this knowledge we are able to give quick insights into more complex models.

Thesis Committee:

Chair:	Dr.ir. Y.M. Dijkstra, Faculty EEMCS, TU Delft
University supervisor:	Dr. J.L.A. Dubbeldam, Faculty EEMCS, TU Delft
Committee Member:	Dr.ir. S. Jain, Faculty EEMCS, TU Delft

Preface

I would like to start of with expressing my appreciation for Dr.ir. Yoeri Dijkstra, my daily supervisor. The weekly meetings where we discussed new results kept me sharp and enthusiastic about what we were doing. His guidance and constructive feedback during the writing process has made the process a lot smoother. Then I would also like to thank my responsible supervisor Dr. Johan Dubbeldam, who during our bimonthly meeting kept both Yoeri and me from losing ourselves in the results. I want to thank Di.ir Jain for being part of my thesis committee.

Lastly I want to thank my family and friends for all their support throughout my life and studies.

Contents

Chapter 1

Introduction

Plankton play a crucial role in Earth's marine ecosystems. They form the base of the ocean food web and significantly influence global biological cycles, producing roughly half of the world's oxygen and absorbing nearly half of its annual carbon dioxide emissions (Basu & Mackey, 2018). Recognizing this importance, there is considerable interest in modeling the complex dynamics of plankton communities to better understand marine ecosystem behavior and how it responds to environmental changes.

However, modeling plankton dynamics is challenging because of the multitude of interacting processes involved (Carlotti, 2019). Many plankton ecosystem models become highly complex, with numerous state variables and parameters, making it difficult to discern how changes in any given parameter affect the outcomes. With today's rapidly changing climate and ocean conditions, this challenge becomes even more pressing: fundamental questions, such as how water temperature or ocean currents alter plankton growth and species composition, remain only partially answered by existing models. Starting an investigation with an overly complex model can be impractical and opaque, often akin to searching for a needle in a haystack. Such an approach requires extensive computation for each small parameter tweak, yet may still fail to reveal the root causes of observed behavior.

In this context, a bottom-up modeling approach is appealing. Instead of beginning with a full-scale, high-detail model, we start with a simpler plankton model that captures the essential processes, and analyze it in depth to reveal underlying dynamics and cause–effect relationships. We then incrementally build up complexity, adding additional species, nutrient types, or processes, to see if and how the behaviors from the simple model carry over to more complex scenarios. Insights gained from the simpler model can ultimately guide where to focus attention in more detailed models. In this research we limit the model to two groups of plankton. The first is phytoplankton (P), this group of plankton is autotrophic, and mostly relies on photosynthesis for energy. Secondly, we consider zooplankton(Z), this group of plankton feeds on phytoplankton. Besides the plankton groups, we have different kinds of nutrients(N), which might or might not be in a viable state for consumption. Figure 1.1 shows a graph of the interactions and general flow of nutrients.

These interactions are modeled using a system of differential equations which have the following rough structure:

$$\begin{aligned} &\textit{change in } P = \textit{grazing of } N - \textit{death of } P - \textit{grazing by } Z \\ &\textit{change in } Z = \textit{grazing on } P - \textit{death of } Z \\ &\textit{change in } N = \textit{death of } P + \textit{death of } Z - \textit{grazing by } P \end{aligned}$$

This formulation omit the feeding of zooplankton on zooplankton, and the state of the nutrients. This general structure already shows the amount of freedom in choosing how each element is formulated. Generally each part of each equation is formulated as a Holling's type equation or a derivative thereof, (Holling, 1959). That is the response is either a linear (Type I), saturating (Type II) or logistic form (Type III). Each form introduces a set of free variables which each tune some behavior, and are generally fitted experimentally.

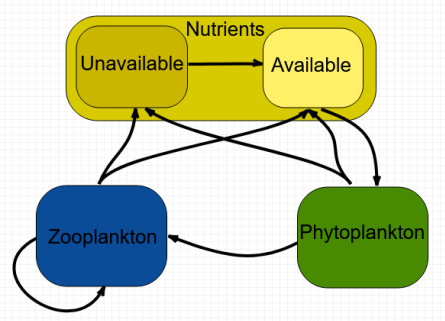

Figure 1.1: Graph showing a high level overview of the flow of interactions

If we remove the dependence on nutrients, and only consider linear responses (Type I). The system reduces to the Lotka–Volterra equations, which model the interaction between a predator and its prey.

$$\begin{aligned} \frac{dP}{dt} &= P(\alpha - \beta Z) \\ \frac{dZ}{dt} &= Z(-\gamma + \delta P) \end{aligned} \tag{1.1}$$

It limits the model to some reproduction rate α, consumption rate β, death rate γ and growth rate δ. There is a rich body of theory analyzing these equations. Classic predator–prey analysis of the Lotka–Volterra system reveals diverse dynamical behaviors as outlined by (Brauer & Castillo-Chavez, 2011): The origin is a saddle point, which is explained by the fact that without prey the predator dies. And without a predator the prey grow unbounded. The system has a stationary point and a conserved quantity. This leads to closed orbits, where prey and predator amounts follow the same orbit indefinitely. While this simple formulation does allow for rigorous mathematical analysis. It already shows a major flaw in the fact that unbounded growth of prey is not physical. For example, a locust swarm will eventually eat so much there is nothing left, and lead to their own demise. One way to repair this problem is by allowing non-linear, or self limiting terms in the growth rate. However, this leads to qualitatively different behavior.

This then leads to a more general formulation which were introduced by (Kolmogorov, 1936):

$$\begin{aligned} \frac{dP}{dt} &= Pf(P,Z), \\ \frac{dZ}{dt} &= Zg(P,Z) \end{aligned} \tag{1.2}$$

Here he stated some conditions on the functions f and g, which need to be satisfied if one would want a realistic predator-prey interaction. These are outlined by (Sigmund, 2007), but the Volterra equations fail to satisfy some of these. (May, 1972) showed how these conditions lead either to stable equilibrium, or to stable limit cycles. Which one of the two was present depended on the choices of parameters. They also stressed how the existence of these limit cycles gave a lot more insight than was previously thought. This gives rise to the need to do a more thorough bifurcation analysis of the system.

The Kolmogorov population model and Lotka-Volterra equations already allows for a model which is applicable, but still mathematically understandable. However, it still lacks to capture nutrient dependency. This is an essential part for a model which can be used to try and get a better understanding of ecological processes. An example of a system of equations which extends the Kolmogorov model is a system proposed by (Steele & Henderson, 1992):

$$\begin{aligned}
\frac{dP}{dt} &= \frac{N}{N+k}\beta P(1-\frac{P}{\gamma}) - Z\lambda\frac{P^n}{P^n+\mu} \\
\frac{dZ}{dt} &= \alpha\lambda\frac{P^n}{P^n+\mu}Z - \delta Z^m \\
\frac{dN}{dt} &= p\,(N_0-N) - \frac{N}{N+k}\beta P(1-\frac{P}{\gamma}) + (1-\alpha)\lambda\frac{P^n}{P^n+\mu}Z
\end{aligned} \tag{1.3}$$

Here they have chosen to set the growth rate of phytoplankton to have a self shadowing part, $\left(1-\frac{P}{\gamma}\right)$, and a nutrient limiting part, $\frac{N}{N+k}$. The nutrient limiting part is a Holling type II reaction. We have that β is the maximal growth rate and k is the half saturation value, that is the value of N for which the growth is half the maximum growth rate. Then we have that the γ gives the value of P for which the death and growth rate would be in balance. The feeding of phytoplankton by zooplankton then follows a response function $\frac{\lambda P^n}{P^n+\mu}$, which is either a Holling type II ($n=1$) or III ($n>1$) reaction. Here λ is the maximum feeding rate, and μ the half saturation value. That means that the actual value of P for for which half the maximum feeding rate is consumed is $\mu^{\frac{1}{n}}$. Of all consumed phytoplankton α is actually converged into zooplankton biomass, so this is the efficiency of the zooplankton. The death rate of zooplankton is given by δZ^m, where $m \in \mathbb{N}$. For $m=1$ we get a straight forward linear death rate, but for higher powers we get a self shadowing effect, which might be due to effects like over population. Lastly the formulation of nutrients is built from three parts. The first is a regenerative part $p(N_0-N)$, which models the entrance of nutrients from outside of the system. Then we have the nutrients eaten by phytoplankton. Lastly is the portion of phytoplankton biomass not converted into zooplankton biomass at consumption. This system becomes closed if $p(N_0-N)=\delta Z^m$. A short analytical analysis of this model can be found in Appendix A.

These three systems show how deep mathematical analysis can be done, but this is mostly due to them all restricting the amount of diversity. They all consider only one type of both zoo- and phytoplankton, but in reality there are whole spectra of species present in eco systems. This means for each individual species there is interactions with

all other species. This aggregation misses the rich diversity of plankton species and their resource specializations. If we attempt to represent multiple phytoplankton species in a purely resource-competition setting, so not considering any zooplankton, classical theory dictates that the number of coexisting species cannot exceed the number of limiting nutrients (Hardin, 1960). In other words, one species will out-compete the others for each resource, eventually dominating. This basic prediction would imply that only a handful of phytoplankton species could coexist on a few nutrients, contradicting the high diversity observed in nature, (Hutchinson, 1961). Researchers have shown that relaxing some assumptions of simple models can resolve this paradox. Notably, (Huisman & Weissing, 1999), demonstrated that when species compete for three or more resources, the system can exhibit oscillatory or chaotic fluctuations that allow many species to coexist on a few resources. In their models, no single species permanently out-competes the others; instead, species abundances cycle in complex ways, preventing competitive exclusion. This result highlights that even deterministic models with simple rules can sustain high biodiversity under non-equilibrium conditions, though the behavior can become difficult to predict or generalize.

Accurately capturing plankton ecosystem requires modeling species diversity. This is where classical models like before fail, they lack the freedom to match measurements. To this end more recent models incorporate multiple plankton functional groups, size classes, or even continuously varying traits. Instead of a single phytoplankton and zooplankton, these models track many types, for example, diatoms vs. picophytoplankton, or small grazers vs. large carnivorous zooplankton, each with distinct parameters for growth, uptake, and predation. This approach can reproduce the coexistence of numerous species observed in real oceans. Plankton Functional Type (PFT) models, for instance, classify organisms into a few broad groups (e.g. nitrogen-fixers, diatoms, copepods) and assign each group unique equations or parameter values. These models brought improved realism, but they were soon criticized for oversimplifying the biological differences within each plankton group. (Anderson, 2005) argued that lumping species into functional categories might overlook important eco-physiological variation. These bigger models also brought another problem, with each addition another set of free parameters emerged. On one hand this created the parameter problem, where chosen values for each would be an impossible task on itself. And as Anderson points out this also brings another problem, where we have so many free variables, that the free variables allow us to fit the model to observed data. But there might be multiple ways to achieve this, then the question arises: which choice reflects reality?

In response, some PFT models were extended to include trait-based details, effectively increasing the number of modeled “species”, this allowed for many parameter combinations. This was done by for example varying parameters over cell size, or optimal water temperature. But while this solved the problem of over simplifying eco-physiological variation, it instead enlarged the parameter problem. (Follows et al., 2007) tackled this emerged ’parameter problem’ by seeding a complex model with many hypothetical phytoplankton types that differed in random physiological traits. In their global ocean simulation, dozens of phytoplankton competitors, with four nutrient types available and

two zooplankton types, were allowed to compete and disperse. Remarkably, about 20 distinct phytoplankton phenotypes emerged as persistent "winners," each dominating in different environmental niches. Top–down control by zooplankton has been shown to be a key factor enabling higher diversity in these complex simulations. Predation can prevent the competitive exclusion of weaker phytoplankton by curbing the abundance of the dominant competitor. As a result, more nutrients remain available in the system, which allows additional species to coexist on what would otherwise be limiting resources. In the example above, the presence of two zooplankton functional groups grazing on the most abundant phytoplankton effectively "freed up" nutrients to support a greater variety of phytoplankton, explaining why 20 species could stably coexist instead of the 16 one might predict from four nutrients in four different climates alone. This is also shown by (Poulin & Franks, 2010). They show how in a size-structured formulation a wide variety of plankton is able to coexist. They argue that resources determine which plankton size classes could exist, while predation determines which ones do exist. In other words, both nutrient supply and grazing pressure are essential for structuring plankton communities, and their balance influences how many species or size classes share the ecosystem.

As another example of a complex model, (Ward et al., 2012) developed a global ocean food-web model that explicitly represents diverse phytoplankton and zooplankton populations distributed across a continuous size range. Their model, which was embedded in a 3D ocean circulation, qualitatively reproduced observed global patterns such as nutrient concentrations and primary production. This success demonstrated that a carefully parameterized trait-based model can achieve both biological realism and consistency with large-scale ocean data. To handle this explosion of parameters, researchers often impose allometric scaling laws, whereby physiological rates are expressed as simple functions of organism size. Many parameters for a given plankton type are determined by its body size according to power-law relationships ($p = aV^b$), rather than tuned individually. This significantly reduces the models degrees of freedom and imposes biologically sensible constraints. Recent evaluations of allometric formulations have found that single traits like cell size can indeed explain a large fraction of variation in plankton functional parameters. In fact, (Andersen & Visser, 2023) showed that size-based trait scaling aligns well with empirical data for processes like nutrient uptake, metabolism, and grazing across plankton taxa.

Allometric scaling usually cannot completely eliminate free parameters, often at least a couple of coefficients must be specified for each relationship, and not all traits scale neatly with size. Andersen notes that even a "size-only" framework needs additional trait axes to accurately capture plankton diversity and ecosystem function. Furthermore, running global simulations or doing sensitivity analyses on such models can be extremely demanding, which makes it difficult to use them for exploring a wide parameter space or for analytical understanding of dynamics.

These two examples already show two different methods to tackle the problem posed by (Anderson, 2005). (Follows et al., 2007) showed how we can increase the number of unique species, while (Ward et al., 2012) instead opted for varying along a trait axis. What both of them also show is that with the exponential increase of parameters another

downside emerges. Highly complex models can behave like “black boxes”, one might trust their output in aggregate, but it is hard to pinpoint cause and effect or to generalize lessons to other systems. This is in stark contrast with the simpler models, where we either have analytical reasons for behavior, or easy access to numerical methods. This black box effect stops us from easily analyzing ”what if” questions, e.g. what if the water temperature increases, what if the gulf stream slows down?

Given these trade-offs, there is growing recognition of the need to bridge the gap between simple and complex models. Rather than treating simple vs. complex as a binary choice, we suppose that we should build the models in a modular fashion: Starting from a core simple model, and then extending it gradually. We then try to see what parts of the structure found at a simpler model carries over. Knowing this might offer some guiding advice on which settings do, and which do not matter when creating a more intricate model. This thesis examines the qualitative bifurcation structure of the size-structured plankton model originally introduced by (Poulin & Franks, 2010). The purpose of this paper is to find out to what extent do the bifurcation layout and stability regimes for a Dirac-delta feeding kernel survive when the kernel is broadened to a finite-width Gaussian?

To answer this, we proceed in two deliberate steps. First, the Dirac-delta version is treated in isolation: Equilibria are derived in closed form, their transcritical and Hopf loci are traced in a two parameter plane. We also investigate the structure of emergent non stationary solutions, to complete the full picture.

Then secondly, we relax the feeding assumption by introducing Gaussian kernels of increasing width and. For each new kernel we repeat the full bifurcation analysis, documenting how the locations and natures of the transcritical, Hopf and torus bifurcations shift relative to the Dirac baseline. For a small deviation we also compare the non stationary behavior and ecological measures.

For all models we also include analysis in the effect of refining, coarsening and extending the chosen discretization. By quantifying these shifts we establish the range for which the simplified model remains a reliable proxy and identify the minimum model complexity required to reproduce ecologically relevant dynamics.

In the methods chapter 2 we first reformulate the used model, after which we discuss the place where we did a simplification. Then we derive analytical solutions of this continuous system. After discretization we can find similar structures, for which we go more in depth. Then we discuss all the setups of the experiments carried out. Finally, we conclude the methods section with a brief outline of the used numerical solver. In the results chapter 3 we will analyze the results outlined in the experimental setup. We present our conclusion in chapter 4, and the discussion of the result in chapter 5

Chapter 2

Method

We start by reformulating the model from (Poulin & Franks, 2010) in section 2.1. Then we discuss two parameter choices in section 2.2, one of which leads to a simplification. This simplification is first analyzed analytically in section 2.3, followed by a discussion of discretization in section 2.4. Then some more analytical work is done on the simplified version of the discretization in section 2.5. In section 2.6 we then give an outline of all different studies conducted in the results chapter 3. We end the chapter in section 2.7 where we discuss what numerical solver we used for the results.

2.1 Model formulation

As a starting point, we take the equations proposed by (Poulin & Franks, 2010). These equations take the following continuous form:

$$\frac{\partial \tilde{P}(s_p)}{\partial t} = \tilde{P}(s_p)\left[\mu(s_p)\frac{\mathcal{N}}{\mathcal{N}+k(s_p)} - \lambda(s_p) - \int_{\mathcal{S}_z} \alpha(s_z,s_p)g(s_z)\frac{\tilde{Z}(s_z)}{F(s_z)+K(s_z)}ds_z\right], \tag{2.1a}$$

$$\frac{\partial \tilde{Z}(s_z)}{\partial t} = \tilde{Z}(s_z)\left[\gamma(s_z)g(s_z)\frac{F(s_z)}{F(s_z)+K(s_z)} - \delta(s_z)\right], \tag{2.1b}$$

$$\mathcal{N}_t = \mathcal{N} + \int_{\mathcal{S}_p} \tilde{P}(s_p)ds_p + \int_{\mathcal{S}_z} \tilde{Z}(s_z)ds_z, \tag{2.1c}$$

$$F(s_z) = \int_{\mathcal{S}_p} \alpha(s_z,s_p)\tilde{P}(s_p)ds_p. \tag{2.1d}$$

Both s_z and s_p are a measure of size for zoo- and phytoplankton respectively. They both take values in a subsets of $\mathbb{R}$ denoted by $\mathcal{S}_z$ and $\mathcal{S}_p$ respectively. Here $\tilde{P}(s_p)$ denote the biomass of Phytoplankton with size s_p, and $\tilde{Z}(s_z)$ is the biomass of zooplankton with size s_z. This quantity behaves like a distribution, where point values have no mass, and to get quantities that would be measurable we would need to integrate over some size interval. We have chosen to use this representation since this representation aligns well with the discretized formulation used later. The first term for the phytoplankton (2.1a)

is a Michaelis–Menten equation and gives the growth due to free nutrients in the system. Here $\mu(s_p)$ is the maximum growth rate, and $k(s_p)$ is the half saturation constant. That is when $\mathcal{N} = k(s_p)$ then we would have half of the maximum growth rate. The second term $\lambda(s_p)$ represent all nutrient losses besides predation by zooplankton. Finally the last term is the amount of phytoplankton of size s_p that gets eaten by all zooplankton. Before considering the terms in this integral we first explain $F(s_z)$ (2.1d). This integral is built up from a feeding kernel $\alpha(s_z, s_p)$, and this represents the preference of a zooplankton of size s_z to consume phytoplankton of size s_p. We set the condition $\int \alpha(s_z, s_p) ds_p = 1$ for all s_z, this is because the constant could be absorbed by scaling K and g in (2.1a) and (2.1b) appropriately and allows us to interpret $F(s_z)$ as the weighted average of the food available for a zooplankton of size s_z. Using this we have for any fixed s_z that $g(s_z)$ is the maximum uptake rate of phytoplankton by zooplankton. And $K(s_z)$ is the half saturation constant, relative to the prey's weighted average availability. Then the total amount of phytoplankton s_p eaten is the weighted integral over these uptake rates. For the zooplankton (2.1b) the first term represent the uptake rate over all phytoplankton. The extra term $\gamma(s_z)$ represents the assimilation and can be seen as how efficient the zooplankton turns phytoplankton biomass into its own biomass. The remaining $1-\gamma(s_z)$ is thus the inefficiency, this term is not present as the system is closed by allowing all losses to be available as free nutrients. Then the last term $\delta(s_z)$, distinct from the Dirac delta function, is biomass losses of zooplankton. To close the system we set the condition that the total nutrients $\mathcal{N}_t$ in the system is the sum of the free nutrients $\mathcal{N}$, the biomass of phytoplankton, and the biomass of zooplankton in (2.1c). An overview is given in Table 2.1.

Variable	Meaning	unit	A_0	e
s_p	Phytoplankton size	μm	-	-
s_z	Zooplankton size	μm	-	-
$\tilde{P}(s_0)$	P biomass per unit size s_0	$\frac{\mu MN}{\mu m}$	-	-
$\tilde{Z}(s_0)$	Z biomass per unit size s_0	$\frac{\mu MN}{\mu m}$	-	-
N	Dissolved nutrients	μMN	-	-
$\mu(s_0)$	uptake rate	day^{-1}	5.9	-0.75
$k(s_0)$	half saturation	μMN	1.0	1.14
$\lambda(s_0)$	Biomass loss	day^{-1}	0.017	-0.6
$g(s_0)$	maximal grazing rate	day^{-1}	7.0	-0.75
$K(s_0)$	half saturation	μMN	1.0	0.24
$\gamma(s_0)$	assimilation	dimensionless	0.7	0.24
$\delta(s_0)$	Biomass loss	day^{-1}	0.17	0.75
$\alpha(s, s_0)$	grazing kernel	dimensionless	-	-

Table 2.1: Table showing the definitions and units of all model variables. Where all variables that are size dependent are denoted as a function of s_0. The values in the rightmost columns are taken from Poulin and Franks (Poulin & Franks, 2010), and are taken unless otherwise specified

In reality we have that all size-dependent parameters are allowed to be any function.

We model them as power-law functions: $v(s) = A_0 s^e$. This is because this narrows the amount of free variables, and has been shown to be generally applicable by (Andersen & Visser, 2023). Where relevant the default values are also shown in Table 2.1.

2.2 Choice of feeding kernel

In section 2.1 we introduced α as the preference of a zooplankton of size s_z to consume a phytoplankton of size s_p. We imposed the condition that the integral over all sizes of phytoplankton for one size of zooplankton would be equal to one. We have not yet specified an exact distribution. In reality this can be of any form, and any continuous probability function would be suitable. We limit ourselves to two distributions. The first is using a Dirac-delta distribution, this is normally denoted as δ, but as this is already a parameter in this system we instead denote it with ρ. This is formulated as $\alpha(s_z, s_p) = \rho(\frac{s_z}{r} - s_p) = r\rho(s_z - r s_p)$. This means that a zooplankton of size s_z exclusively consumes phytoplankton of size $\frac{s_z}{r}$. In reality the amount of phytoplankton of exactly size s_p would be most likely be non-existent. So physically this distribution does not make a lot of sense. However, it simplifies the differential equations, and allows a useful exercise, which we will show in section 2.3. Using ρ we have that equation (2.1) reduces to:

$$\frac{\partial \tilde{P}(s_p)}{\partial t} = \tilde{P}(s_p)\left[\mu(s_p)\frac{\mathcal{N}}{\mathcal{N} + k(s_p)} - \lambda(s_p) - g(r s_p)\frac{\tilde{Z}(r s_p) r}{\tilde{P}(s_p) + K(r s_p)}\right]. \tag{2.2a}$$

$$\frac{\partial \tilde{Z}(s_z)}{\partial t} = \tilde{Z}(s_z)\left[\gamma(s_z) g(s_z)\frac{\tilde{P}(\frac{s_z}{r})}{\tilde{P}(\frac{s_z}{r}) + K(s_z)} - \delta(s_z)\right]. \tag{2.2b}$$

$$\mathcal{N}_t = \mathcal{N} + \int_{\mathcal{S}_p} \tilde{P}(s_p) ds_p + \int_{\mathcal{S}_z} \tilde{Z}(s_z) ds_z. \tag{2.2c}$$

The second kernel we choose is a normalized normal distribution, i.e.:

$$\begin{aligned} \alpha(s_z, s_p) &= \frac{1}{c(s_z)\sqrt{2\pi\sigma^2}} \exp\left(-\frac{(s_p - \frac{s_z}{r})^2}{2\sigma^2}\right). \\ c(s_z) &= \int_{\mathcal{S}_p} \frac{1}{\sqrt{2\pi\sigma^2}} \exp\left(-\frac{s_p - \frac{s_z}{r}}{2\sigma^2}\right) ds_p. \end{aligned} \tag{2.3}$$

This is chosen because this might simulate how a zooplankton individual of size s_z prefers to eat a phytoplankton of size s_p, but by random chance also eats larger and smaller phytoplankton. Because the causes of these effects are assumed to be random, we also have that by the central limit theorem the average pattern would resemble a Gaussian distribution. Another benefit is that the Dirac-delta distribution can be seen as the limit of a normal distribution as the standard deviation goes to 0. The only problem with this distribution is that both tails extend to infinity, so to satisfy our distribution constraint need to normalize it back with the integral over all s_p.

2.3 Continuous Analytical solutions

Before analyzing the discretized systems we take a step back to the continuous formulation with the Dirac-delta feeding kernel seen in equation (2.2).

In the following the relation $s_z = rs_p$ holds, and are used interchangeably to make it clear which variable, belongs to which group. Furthermore the following cases hold pointwise, and so a global solution is build from a combination of these. Some global restrictions follow after. For both $\tilde{P}(s_p)$ and $\tilde{Z}(s_z)$ we either have that they are zero or non zero. That means there are 4 cases to be studied: The first is the trivial solution where $\tilde{P}(s_p) = \tilde{Z}(s_z) = 0$. The second is where $\tilde{Z}_i(s_z) \neq 0$ and $\tilde{P}(s_p) = 0$, this is clearly not possible by equation (2.2b). The first interesting case is where $\tilde{P}(s_p) \neq 0$ and $\tilde{Z}(s_z) = 0$. From equation (2.2a) it follows that:

$$\mathcal{N} = \frac{\rho(s_z)k(s_p)}{\mu(s_p) - \lambda(s_z)}. \tag{2.4}$$

But we get no further information on the value $\tilde{P}(s_p)$. What we do note here that if there are multiple s_p which fall into this case, then all these need to equate to the same expression. The final case is where they both are nonzero, for this we see that:

$$\tilde{P}(s_p) = \frac{\delta(s_z)K(s_z)}{\gamma(s_z)g(s_z) - \delta(s_z)}. \tag{2.5a}$$

$$\tilde{Z}(s_z) = \frac{\tilde{P}(s_p) + K(s_z)}{rg(s_z)} \left(\mu(s_p) \frac{\mathcal{N}}{\mathcal{N} + k(s_p)} - \lambda(s_p) \right) \tag{2.5b}$$

As was already said earlier these are pointwise results, and any combination is possible. The only remaining constraint is that equation (2.2c) is satisfied, and $\mathcal{N}_t$ can be chosen accordingly. If any point falls into the third case then all values can be calculated, and the validity depends on the last equation. If we do not have any in the third case then we generally do not have a solution yet. For this we have 2 possibilities, the first is we fix $\mathcal{N}$ to some value. The second is that we instead for some $\hat{s}_z$ fix $\tilde{Z}(s_z)$. Then it follows that:

$$\mathcal{N} = \frac{\rho(\hat{s}_z)k(\hat{s}_p)}{\mu(\hat{s}_p) - \rho(\hat{s}_z)}. \tag{2.6}$$

$$\rho(\hat{s}_z) = \lambda(\hat{s}_p) - \frac{rg(\hat{s}_z)\tilde{Z}(\hat{s}_z)}{\tilde{P}(\hat{s}_p) + K(\hat{s}_z)}. \tag{2.7}$$

$$= \lambda(\hat{s}_p) - \tilde{Z}(\hat{s}_z) \left(\frac{rg(\hat{s}_z)}{K(\hat{s}_z)} - \frac{r\delta(\hat{s}_z)}{\gamma(\hat{s}_z)K(\hat{s}_z)} \right). \tag{2.8}$$

Some conditions follow if we would want all quantities to be physical, and are only relevant when their respective solution is valid. We assume that all parameters remain strictly positive, then the first condition follows from equation (2.5a), and is that $\gamma(s_z)g(s_z) > \delta(s_z)$. Likewise the second follows from equation (2.6) and is that

$\mu(\hat{s}_p) > \rho(\hat{s}_z)$. The third follows from (2.8) and is that $\lambda(\hat{s}_p) > \frac{rg(\hat{s}_z)\tilde{Z}(\hat{s}_z)}{\tilde{P}(\hat{s}_p)+K(\hat{s}_z)}$ The last is from equation (2.5b) and is that $\mathcal{N} > \frac{\lambda(s_p)k(s_p)}{\mu(s_p)-\lambda(s_p)}$.

An interesting case arises if we let $\mathcal{I} = \{s_p; \tilde{P}(s_p) \neq 0\}$ and $\mathcal{J} = \{s_p \in \mathcal{I}; \tilde{Z}(rs_p) \neq 0\}$, and $\mathcal{I} \backslash \mathcal{J} \neq \varnothing$, that is there are some s_p for which $\tilde{P}(s_p)$ has no predation. Then we can use these $\hat{s}_p \in \mathcal{I} \backslash \mathcal{J}$, to find $\mathcal{N}$ using equation (2.4). But this then means that with the third condition that for all $s_p \in \mathcal{J}$:

$$\frac{\lambda(\hat{s}_p)k(\hat{s}_p)}{\mu(\hat{s}_p)-\lambda(\hat{s}_p)} > \frac{\lambda(s_p)k(s_p)}{\mu(s_p)-\lambda(s_p)}. \tag{2.9}$$

This means that for all $\hat{s}_p \in \mathcal{I} \backslash \mathcal{J}$ that this expression needs to be the maxima over all $s_p \in \mathcal{I}$. Further more they all need to be exactly equal.

The fixing of some $\tilde{Z}$ might seem like a useless exercise, but a useful case of this is if we let $\mathcal{I} = [s^-, s^+]$ for $s^- < s^+ \in \mathbb{R}$ and $\mathcal{J} = [s^-, s^+)$. That is there is some range of sizes for there exist phytoplankton, and at the maximum size the zooplankton reaches zero. Now in this case if we would increase $\mathcal{N}_t$ one of two things can happen: The first is that $\tilde{Z}(s^+)$ increases but $\mathcal{I}$ stays unchanged, physically this can be thought of that the size limit is reached. The second case is that s^+ increases, this then can be thought of that more food allows for bigger plankton species. For this second case we would still need the maximum constraint (2.9) to hold, and so because s^+ can be increased arbitrarily we require $\mathcal{N}$ to increase monotonically with s^+. Of course a combination of these two can hold as well where s^+ can only increase till an absolute maximum, then the monotonicity only needs to hold from s^- till this maximum.

If we would have chosen the parameters in a less restricted fashion we can also choose the parameters in such a way that $\tilde{P}(s^-) = \tilde{P}(s^+) = \tilde{Z}(rs^-) = \tilde{Z}(rs^+) = 0$. For example, this can be achieved by letting $\mathcal{I} = [1, 2]$ and setting all parameters to be constants except $K(s_z) = -(s_z - 1.5)^2 + 0.25$ and $k(s_p) = (s_p - 1.5)^2$.

2.4 Discretization

We discretize the size ranges into size classes, that is we let $\mathcal{S}_p = \bigcup_i s_p^i$, and $\mathcal{S}_z$ is discretized analogously. Now for all size classes we discretize all continuous parameters of equation (2.1) by taking point values. That is for each size class we take some value $\hat{s}_{p/z}^i \in s_{p/z}^i$, then for all free variables we let $a_i = A_0(\hat{s}_{p/z}^i)^e$. We let $\Delta s_p^i = \max(s_p^i) - \min(s_p^i)$, that is the width of size class s_p^i, and Δs_z^j is done analogously. We let $\tilde{P}_i = \frac{1}{\Delta s_p^i} \int_{s_p^i} \tilde{P}(s_p) ds_p$,

and again $\tilde{Z}_i$ in the same way. Then the discretization of equation (2.1a) is as follows:

$$\begin{aligned}\frac{dP_i}{dt} &= \frac{d}{dt}\frac{1}{\Delta s_p^i}\int_{s_p^i}\tilde{P}(s_p)ds_p.\\ &= \frac{1}{\Delta s_p^i}\int_{s_p^i}\tilde{P}(s_p)\left[\mu(s_p)\frac{\mathcal{N}}{\mathcal{N}+k(s_p)} - \lambda(s_p) - \int_{\mathcal{S}_z}\alpha(s_z,s_p)g(s_z)\frac{\tilde{Z}(s_z)}{F(s_z)+K(s_z)}ds_z\right]ds_p.\\ &\approx \tilde{P}_i\left[\mu_i\frac{\mathcal{N}}{\mathcal{N}+k_i} - \lambda_i - \sum_j a_{ij}g_j\frac{Z_j\Delta s_z^j}{F_j+K_j}\right].\end{aligned}$$

Here we assumed that $\tilde{P}$ is smooth enough to interchange the derivative and the integral. For equation (2.1b) a similar thing can be done. Taking everything together we get:

$$\frac{d\tilde{P}_i}{dt} = \tilde{P}_i\left[\frac{\mu_i\mathcal{N}}{\mathcal{N}+k_i} - \lambda_i - \sum_j \alpha_{ij}g_j\frac{\tilde{Z}_j\Delta s_j^z}{F_j+K_j}\right]. \tag{2.10a}$$

$$\frac{d\tilde{Z}_j}{dt} = \tilde{Z}_j\left[\frac{\gamma_j g_j F_j}{F_j+k_j} - \delta_j\right]. \tag{2.10b}$$

$$\mathcal{N}_T = \mathcal{N} + \sum_i \tilde{P}_i\Delta s_i^p + \sum_j \tilde{Z}_j\Delta s_j^z. \tag{2.10c}$$

$$F_j = \sum_i \alpha_{ij}\tilde{P}_i\Delta s_i^p. \tag{2.10d}$$

Throughout the remainder of this work we will frequently will talk about a species being the largest present. We adopt the ordering of species $\tilde{P}_1 < \tilde{Z}_1 < \tilde{P}_2 < \tilde{Z}_2 < \dots$ and use expressions like "$\tilde{P}_i$ is the largest present" to mean that both $\tilde{P}_j, \tilde{Z}_j > 0$ for $j < i$, and $\tilde{Z}_i = 0$.

The choice of discretization of α remains free, if we want to find the straight forward discretized version of equation (2.2), we require that $s_z^i = rs_p^i$. This then means that $\Delta s_z^i = r\Delta s_p^i \hat{=} r\Delta s_i$. Then we set $\alpha_{ij} = 0$ for all $i \neq j$, this makes the sum in equation (2.10a) disappear. Then for $i = j$ we let $\alpha_{ij} = \frac{1}{\Delta s_i}$, this is because we want to get rid of the size class dependence in equation (2.10d). This leads to the following system:

$$\frac{\partial\tilde{P}_i}{\partial t} = \tilde{P}_i\left[\mu_i\frac{\mathcal{N}}{\mathcal{N}+k_i} - \lambda_i - g_i\frac{\tilde{Z}_i r}{\tilde{P}_i+K_i}\right]. \tag{2.11a}$$

$$\frac{\partial\tilde{Z}_i}{\partial t} = \tilde{Z}_i\left[\gamma_i g_i\frac{\tilde{P}_i}{\tilde{P}_i+K_i} - \delta_i\right]. \tag{2.11b}$$

$$\mathcal{N}_t = \mathcal{N} + \sum_i \left(\tilde{P}_i + \tilde{Z}_i r\right)\Delta s_i. \tag{2.11c}$$

It can be seen that this indeed is a straight discretization of system (2.2). To formalize this, we can also reach this α_{ij} if we would have set $\alpha_{ij} = \frac{1}{r\Delta s_i\Delta s_j}\int_{rs_i}\int_{s_i}\delta(s_p - \frac{s_z}{r})ds_p ds_z$. That is the average over the region $s_i \times rs_j$.

Now for the gaussian of equation (2.3) we discretize as:

$$\alpha_{ij} = \frac{1}{c(\hat{s}_z^j)} \frac{1}{\Delta s_p^i} \int_{s_p^i} \frac{1}{\sqrt{2\pi\sigma^2}} \exp\left(-\frac{(s_p - \frac{\hat{s}_z^j}{r})^2}{2\sigma^2} \right) ds_p \tag{2.12}$$

.

That is, for any size class of zooplankton, we take for each phytoplankton size class the average of the continuous feeding kernel at $\hat{s}_z^j \in s_z^j$. Here, $\hat{s}_z^j$ is taken as the midpoint of size class s_z^j.

In Figure 2.1 we can see evaluations of equation (2.12) for a range of σ. Where $\Delta s = \frac{1}{8}$ and $r = 1$, on the vertical axes we have one row per $\tilde{Z}_i$ and each column represent $\tilde{P}_i$. It is obvious that if we take σ sufficiently small that the resulting α would be such that the system reduces to the found Dirac delta formulation. For larger σ we can see that there is large overlap in the preference of different $\tilde{Z}_i$, and the system is expected to be quite different from the Dirac delta formulation. But in between it is expected that the system will behave quite similar.

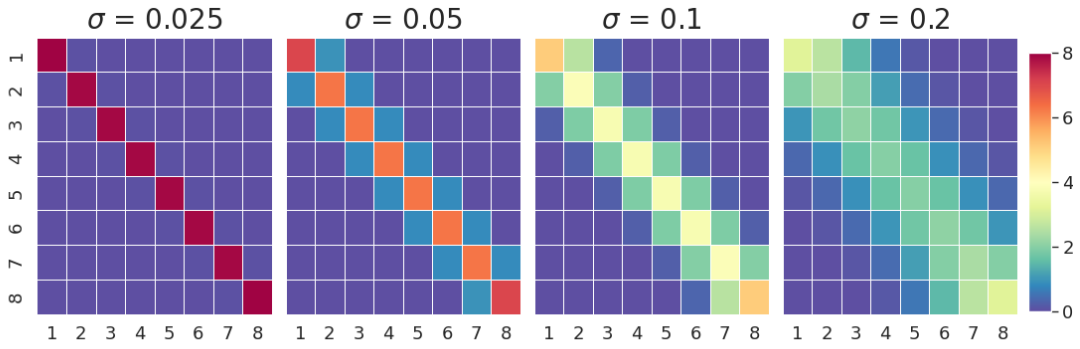

Figure 2.1: Four plots showing the kernel α_{ij} for different values of σ. The vertical axes gives j, and the horizontal i. That is a single row represents the preference of $\tilde{Z}_j$ for different $\tilde{P}_i$.

2.5 Discretized analytical solutions

For the discretized system (2.11), which is the discretization of the Dirac-Delta system (2.2), we follow an analogous analysis as was done in section 2.3.

That is we consider possible solutions per size class pair. Again there is 4 combinations. The first being the trivial solution. Again there can be no zooplankton without phytoplankton, so the second case is not possible. Then the third case, in which $\tilde{P}_i \neq 0$, while $\tilde{Z}_i = 0$. This gives us the following expression:

$$\mathcal{N}_i \equiv \frac{\lambda_i k_i}{\mu_i - \lambda_i}. \tag{2.13}$$

Again $\tilde{P}_i$ remains unknown, but here again we have that if multiple i fall in this category, then they all must equate to the same $\mathcal{N}$. Then the last case in which they both are nonzero. This gives:

$$\tilde{P}_i = \frac{\delta_i K_i}{\gamma_i g_i - \delta_i} \equiv \mathcal{P}_i \tag{2.14a}$$

$$\tilde{Z}_i = \frac{\tilde{P}_i + K_i}{r g_i} \left(\frac{\mu_i \mathcal{N}}{\mathcal{N} + k_i} - \lambda_i \right). \tag{2.14b}$$

It is most obvious that these 4 are the same as found for the continuous system in section 2.3. Just like there we again have that either for some i we have the third case, or $\mathcal{N}$ remains unknown. Again we can fix it to some value or instead for any i fix $\tilde{Z}_i$. This then gives us:

$$\begin{aligned} \mathcal{N} &= \frac{\rho_i k_i}{\mu_i - \rho_i}. \\ \rho_i &= \lambda_i - \frac{r g_i \tilde{Z}_i}{\tilde{P}_i + K_i}. \end{aligned} \tag{2.15}$$

The constraints ensuring non-negativity of all quantities follow analogously To reiterate: $\gamma_i g_i > \delta_i$, $\mu_i > \rho_i$, $\lambda_i > \frac{r g_i \tilde{Z}_i}{\tilde{P}_i + K_i}$ and $\mathcal{N} > \frac{\lambda_i k_i}{\mu_i - \lambda_i}$.

Again a similar interesting case arises, where we take $\mathcal{I} = \{i; \tilde{P}_i \neq 0\}$ and $\mathcal{J} = \{i \in \mathcal{I}; \tilde{Z}_i \neq 0\}$ with $\mathcal{I} \backslash \mathcal{J} \neq \varnothing$. That is there a set of present phytoplankton, of which a subset has a zooplankton that eats them. From this we can use equation (2.13). Which again means that for $i \in \mathcal{I} \backslash \mathcal{J}$ $\mathcal{N}_i$ needs to be the same, and the maximum over all $i \in \mathcal{I}$. The only remaining unknowns are $\tilde{P}_i$ for $i \in \mathcal{I} \backslash \mathcal{J}$, the only remaining constraint we have is that:

$$\sum_{i \in \mathcal{I} \backslash \mathcal{J}} \tilde{P}_i \Delta s_i = \mathcal{N}_t - \mathcal{N}_i - \sum_{i \in \mathcal{J}} (\tilde{P}_i + r \tilde{Z}_i) \Delta s_i. \tag{2.16}$$

Now if for some $n \in \mathbb{N}$ we let $\mathcal{I} = \{1, \dots n\}$ and $\mathcal{J} = \{1, \dots n-1\}$ for $n > 1$ or $\mathcal{J} = \varnothing$ for $n = 1$, some interesting structure follows. First of we have that for all $i \in \mathcal{J}$ that equation (2.14a) holds. Secondly we have that equation (2.13) for n holds, which gives us all $\tilde{Z}_i$ by (2.14b). For all $i \notin \mathcal{I}$ we have that $\tilde{P}_i = 0$, and thus $\tilde{Z}_i = 0$. The only remaining unknown is $\tilde{P}_n$, this follows from equation (2.11c):

$$\tilde{P}_n \Delta s_i = \mathcal{N}_t - \mathcal{N} - \sum_{i < n} (\tilde{P}_i + r \tilde{Z}_i) \Delta s_i. \tag{2.17}$$

Interestingly this is a linear equation in $\mathcal{N}_t$. Two points of interest occur on this line, the first where $\tilde{P}_n = 0$, and the second where $\tilde{P}_n = \mathcal{P}_n$. That is the nutrient value for which the size class starts existing, and the value where it saturates. Now this n was arbitrary, and we denote the family of these sets $\mathcal{I}$ and $\mathcal{J}$ with $\mathbf{P}$. Between any consecutive members of $\mathbf{P}$ there exists some other solution, these solutions have $\mathcal{I} = \mathcal{J}$. For these solutions all $\tilde{Z}_i$ remain free and one can be chosen to be fixed to any value, as long as the constraints are hold. This family of solutions is denoted by $\mathbf{Z}$. Now using these two families we can create a path of solutions, starting with no nutrients $\mathcal{N}_t = 0$. No nutrients

means no food for phytoplankton, which in turn means no food for the zooplankton, thus the starting point is the trivial solution. Now we increase $\mathcal{N}_t$, and with this increase we get that the first member of $\mathbf{P}$, which is just $\tilde{P}_1$, increases following equation (2.17). At some point $\mathcal{N}_t$ is such that $\tilde{P}_1 = 0$, this means that the trivial solution crosses over the first and we start following this first member instead. Further increase leads to the point where $\tilde{P}_1 = \mathcal{P}_1$. This point also lies in the first member of $\mathbf{Z}$, with $\tilde{Z}_1 = 0$. Now we step onto this first member and increase $\tilde{Z}_1$. To see how far this increase is we have to look at the second member of $\mathbf{P}$. Here we know the value of $\tilde{Z}_1$, and for which $\mathcal{N}_t$ we have that $\tilde{P}_2 = 0$. So we can increase $\tilde{Z}_1$ from 0 till this other value, and we cross over the second member of $\mathbf{P}$. This pattern can be repeated until all size classes for both groups are present, at which point the only remaining thing that can be done is increasing $\tilde{Z}_n$.

An interesting parallel to section 2.3 can be made here. There we found that with increasing $\mathcal{N}_t$ we have two choices, either allow for larger plankton species, or increase the largest zooplankton. The discrete solution back and forth found here is following the first case, while if each size class is present we follow the second.

In Figure 2.2 we can see these two families of solutions. Not the whole range of $\mathcal{N}_t$ is shown for each, but only the part where they are relevant. Here we have that $n = 8, \Delta s_i = \frac{1}{8}, s^- = 1$, for a range of $\mathcal{N}_t$ on the horizontal axes. We changed the scaling parameter of δ_0 to -1.5, this is done because for the value from Table 2.1 we get that all $\mathcal{P}_i$ are almost identical. We can see that these solution families indeed match up nicely. The parts of $\mathbf{P}$ have that everything is stationary except for $\tilde{P}_i$, which increases linearly. The parts of $\mathbf{Z}$ wee see that all $\tilde{Z}_i$ increase in unison, creating a staircase like pattern. Here we note that while this structure builds up from the ground up nicely, it is not the only set of solutions that exist. We can for instance create the exact same structure, but then with families without $\tilde{P}_1$, which start with $\tilde{P}_2$. This is not the only example, as these structures can be made using any subset of i. Besides these 'nice' structures a whole range of irregular structures can be made as well, where the order is random. To see that in our case this nice structure is actually interesting we have to look into the stability, which will be done in section 3.1. But all of these intersections are transcritical bifurcations, so we expect that if they are non degenerate, that stability carries over from one to the next solution. By analogous reasoning to the continuous case, we have that for this structure to be physical that the expression for $\mathcal{N}$ needs to monotonic in i.

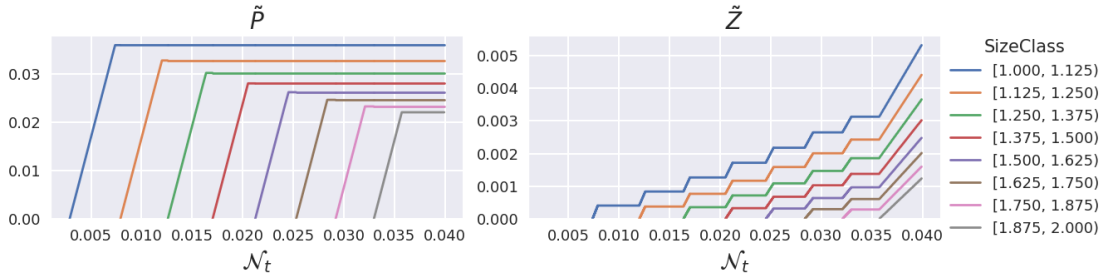

Figure 2.2: Two figures showing values for different values of $\mathcal{N}_t$. The left showing Phytoplankton size classes and the right Zooplankton size classes

2.6 Experimental setup

All experiments below will unless stated explicitly otherwise use the parameter value from Table 2.1, where we use the lower bound of each size class for $\hat{s}^i_{p/z}$. Experiments will be carried out with eight size classes of equal size on the interval $\mathcal{S} = [1, 2]$. The reason for eight size classes is that it allows straight forward comparison between halving the number of size classes multiple times while keeping the size classes equal in width. We did not choose 16, as this then posed more numerical challenges for the experiments done for the more general kernel. r was kept equal to 1.

Now we start the result in section 3.1 where we first analyze the stability of the already found family of solutions of section 2.5. The stability of these solutions follows from analyzing the Jacobian. This Jacobian is readily available for system (2.11), so can be evaluated easily. The stability follows from the eigenvalues of this Jacobian, and if all eigenvalues have real part less than zero, than the solution is said to be stable, and unstable if not. Stability means that if we start in some (small) region around this point we have that overtime we converge to this point. If a system is unstable then we get that no matter how close we start to this point we get pushed away from it over time, and only if you are on the exact value will it actually be stationary. We do refer to literature like (Strogatz, 2000) for further explanation, and some mathematical rigor behind this imprecise explanation. The Jacobian, and its eigenvalues are calculated using numpy. We are interested in the stability as these act as a sink, solutions that start close enough will, given enough time, converge to these points. In reality $\mathcal{N}_t$ might not be constant, but might be swaying up and down with the seasons, what we then have is that the sink constantly moves, and the values follow this movement with some lag.

We investigate these solutions using some elementary bifurcation theory, in particular we will show how the interaction of the two families found in the tail part of section 2.5 leads to the found stability. We forgo some rigor behind the statements made, but instead refer the reader to literature like (Seydel, 2010). The reason we also want the parts in between the already found analytical solutions is that we than can say how larger size classes potentially enter, or leave the system.

In coupled systems like these it is not surprising to find that solutions are generally not stationary, and instead oscillate over time. That is why in section 3.2 we take a small detour into limit cycles. These limit cycles follow from Hopf-bifurcation found in section 3.1.

We have copied the parameter values of Table 2.1 blindly from (Poulin & Franks, 2010). But these values might or might not be correct, that is why we extend the study into two parameters in section 3.3. In this study we follow the encountered Hopf-bifurcation with δ_0 also being a free parameter. δ_0 was chosen as this was the parameter studied by (Steele & Henderson, 1992), and it is generally chosen as a closure of the system, as this parameter is hardest to give a concrete value. Here we then also show how the found structure changes under different choices of discretization, by halving and doubling Δs, and by doubling the number of size classes.

This study is continued in section 3.4, where for two parameters we investigate stable

limit cycles. Beyond the stable limit cycles we investigate behavior after time integrating. For this we first spread half of the biomass evenly over all species, and then integrating for 10^5 days. 10^5 is chosen as this gives time for species to die out, as the maximum rate at which $\tilde{P}_i$ and $\tilde{Z}_i$ die is λ_i and δ_i respectively. That is, if they are without any nutrients, then $\tilde{Z}_i = ce^{-\delta_i t}$, which with numerical precision will be 0 given sufficient time. After this the system is time integrated another 500 days, and a species is said to remain if over this period the maximum value exceeds 10^{-18}.

Then we continue to the system (2.12). This is done for $5\sigma = \Delta s_i = \frac{1}{8}$. This is chosen as the resulting α is close to being in a form such that the system almost reduces to system (2.11), as shown in Figure 2.1. This then is done in the hope that some behavior previously found carries over. We repeat the same steps as the other system. That is, we start of by finding the full solution in section 3.5, we then also take a look into the emergent stable limit cycle in section 3.6. For this system we also do a two parameter study in line with section 3.3 in section 3.7. And take a look into time dependent solutions in section 3.8 The last experiments done in section 3.9 is repeating the stationary parts of the study, but then for $\sigma \in \{\frac{2}{5}\Delta s_i, \frac{4}{5}\Delta s_i, \frac{8}{5}\Delta s_i\}$. This is done to see how far we can push the discretized kernel before the structure breaks down.

We then gather all information in section 3.10 and compare the results side by side, and identify where behavior carries over, and where it does not. We also outline how these results might be used to identify where interesting behavior might occur.

In section 3.11 we transform the previously gotten results into values which are more directly interpretable. The first value we will look into is the biomass of the system, the values thus far have been biomass per size class, so the biomass will be $\sum_i (\tilde{P}_i + r\tilde{Z}_i)\Delta s_i$. By equation (2.11c) this is equal to $\mathcal{N}_t - \mathcal{N}$. Because we investigate the impact of changing $\mathcal{N}_t$ we instead look at the biomass as a percentage of the total nutrients, i.e. $1 - \frac{\mathcal{N}}{\mathcal{N}_t}$, this will be called the efficiency, as this shows how much of the available nutrients are utilized. The second quantity we will look at is the primary production, this is how much inorganic matter is transformed into biomass. For our models this equates to:

$$\sum_i \tilde{P}_i \frac{\mu_i \mathcal{N}}{\mathcal{N} + k_i} \tag{2.18}$$

This is given as a rate per day. For the stationary parts these quantities are readily available. For the non stationary parts this will be taken as the average over 500 days, after the system has settled.

Because the choice of δ_0 is rather arbitrary, and all values were blindly copied, we present an interactive tool to quickly explore other parameters besides δ_0 in section 3.12. This allows to quickly check a lot of combinations, and see which might have structures worthy of a more in-depth analysis.

2.7 Auto-07p

For all the numerical solutions we used Auto-07p, which is publicly available software for continuation of ODE's. (Oldeman et al., 2007). The software uses Newton-Raphson

iterations with a pseudo-arc length method to continue the found solutions. It allows the detection of a wide variety of bifurcation types.

Auto uses user defined C functions which define the system of ODE's. The used files can be found in appendix A.2. We made use of the built in numerical approximation of the jacobian. Both because it gave better convergence, and in the case of the more general feeding kernel the analytical expression becomes cumbersome, and mistakes are made easily. All constants that are not problem specific are kept on the suggested values from the manual. The only constants varied were the amount of dimensions to change the amount of size classes. The arc-length was also not constant for each worked out case. Throughout the problems it changed to find values which converged, were able to find all needed bifurcations, but were also big enough to compute all solutions quickly. The general range of values can be found in appendix A.3.

With the base version of auto all solutions should be able to be found. But the base version only prints six variables, some tricks using PVLS subroutines can be used to print the remaining, but this requires custom code each time the number of size classes are changed. Instead, we modified the source code as suggested by (Eedara, 2016), to alter Auto's output behavior. Note that this does nothing to the solution algorithms and is only done for debugging purposes.

Most of this work has been done manually in the Auto command line user interface (CLUI). But afterwards we were able to create scripts which achieved the same results. The skeleton of these scripts and some notes on how to adept them can be found in appendix B.

Chapter 3

Results

We will start the results in section 3.1 by analyzing the stability of the previously found solution. Following this we will examine emergent limit cycles in section 3.2. We then conduct a two parameter study for both the stationary solutions, in section 3.3, and the limit cycles, in section 3.4. We continue with system (2.10), with α from equation (2.12). In section 3.5 we first find the stable stationary solutions for a range of $\mathcal{N}_t$. We then also perform a two parameter study on this system, and see how discretization choices affect the behavior in section 3.7. For the standard discretization we investigate stable limit cycles in two parameters in section 3.8. We finish the results for system (2.10) in section 3.9 where we see how choices of σ affect both the solutions, and the regions in two parameters. The results of these two systems are then compared in section 3.10. We aim to identify where they share, and where the do not share, behavior. In section 3.11 we look into two ecological measures, the first being biomass and the second the primary production. Then we conclude the results in section 3.12 where we discuss a tool useful for doing a quick analysis.

3.1 Dirac-Delta kernel stability

In Figure 3.1a we show the largest real part among the eigenvalues of the trivial solution and the first four members of both **P** and **Z**. Solid lines denote members of **Z**, while dotted lines denote members of **P**. It can be seen that at each transition point one of the eigenvalues has a rapid increasing real part, whereas for the next solution the maximal real part drops quickly. This links the stable parts together, and thus the found solution path in section 2.5 is stable the whole way. We also find that the stability transfers, so this allows us to conclude that the following happens: As we have already noted in section 2.5 there are two families of solutions at play **P** and **Z**. We start with the trivial solution in $\mathcal{N}_t$ and this was stable as seen in the previous section. The trivial solution can be seen as a part of **Z**. The first member of **P**, that is the one where only $\tilde{P}_i \neq 0$, will start off with $\tilde{P}_1 < 0$. With increasing $\mathcal{N}_t$, this increases linearly. Eventually $\tilde{P}_1$ reaches 0 and thereafter becomes positive This means that this solution branch, will crosses the stable trivial solution. This is a transcritical bifurcation, and if it is nondegenerate, then

the stability will transfer. This is indeed what we found. Then we continue along the blue line shown in Figure 2.2 until $\tilde{P}_1 = \mathcal{P}_1$. At this point we again cross a member of **Z** as explained in section 2.5. This then again is a transcritical bifurcation, and again if nondegenerate the stability will transfer. It again crosses over the next member of **P**, and again it is a nondegenerate transcritical bifurcation, and the stability transfers back to the next member of **P**. Repeating this argument along the branch shows that no additional bifurcations are encountered, as the whole path remains stable. Here we note that we may have stepped over two bifurcations simultaneously without noticing, but then these solutions must live on a region so small that for the larger picture they can be neglected.

These flat parts of the members of **P** are not the eigenvalues that rapidly increase or decrease, but what can be noted is that they slowly approach 0. In Figure 3.1b we can see that this trend continues, and at $n = 123$ it crosses zero, indicating that between these 2 families there is no stable solution left.

If we instead of adding larger groups we increase $\mathcal{N}_t$ we have that one pair of complex eigenvalues slowly moves closer to 0, and at some point goes over. This means that a Hopf bifurcation is encountered, which will be further explored in section 3.2.

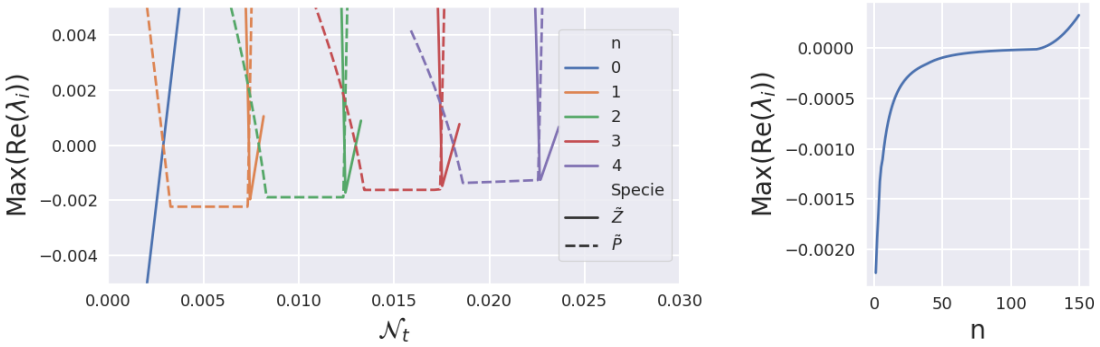

(a) A plot showing the maximum of the real parts of the eigenvalues for members of **P**, member of **Z**, and the trivial solution.

(b) A plot showing the largest real part among the eigenvalues of **P** for n

Figure 3.1: two plots about the stability of members of **P**, **Z** and the trivial solution.

3.2 Dirac-Delta kernel Limit cycles

In the previous section we found the stable branches with increasing $\mathcal{N}_t$ until all size classes were present. If we further increase $\mathcal{N}_t$ till $8.21 * 10^{-2}$ we find a Hopf bifurcation. From this Hopf bifurcation we are able to switch onto a stable limit cycle. This limit cycle starts with low amplitude oscillations and slowly increases in amplitude. Some of these are shown in Figure 3.2. For each pair the general structure is as follows: First the phytoplankton increases in value, this increase is followed a little later by zooplankton. The rise in zooplankton then means that more phytoplankton is being consumed and the concentration drops again. This drop is then followed by zooplankton unable to

sustain their numbers due to a decrease in food. For $i = 1$, we can see that before this drop the phytoplankton regenerates a little bit, but ultimately falls again. This second part is explained by the interconnection of all systems, and while $\tilde{P}_1$ drops, so do the others, this in turn makes it so that more nutrients are available, allowing $\tilde{P}_1$ to resist the pressure from the increased $\tilde{Z}_1$.

With increasing $\mathcal{N}_t$ it can be seen that for phytoplankton the cycles stay around $3.6 * 10^{-2}$, but the amplitude increases. For the zooplankton we see that the mean level around which the cycles oscillate increases, this is in line with the underlying, now unstable, stationary structure. These stable limit cycles reach a torus-bifurcation at $\mathcal{N}_t = 9.6 * 10^{-2}$, after which the structure remains unknown.

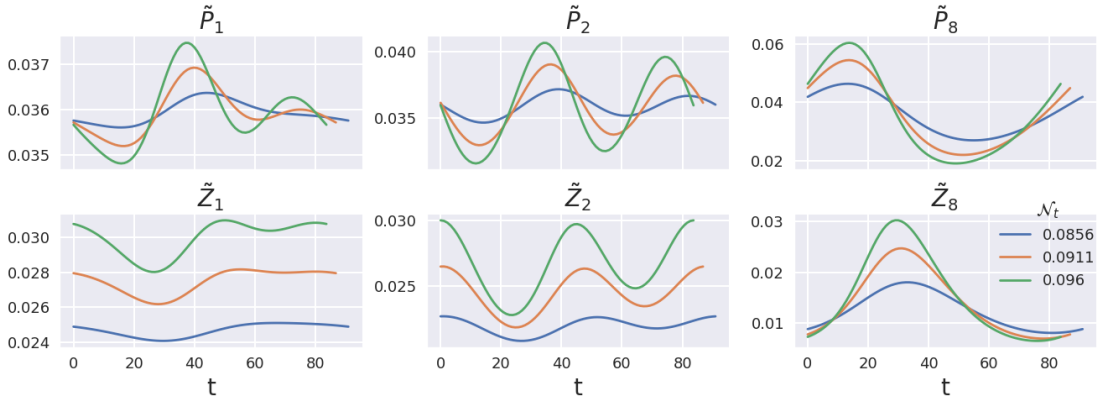

Figure 3.2: Stable limit cycles of $\tilde{P}_i$ and $\tilde{Z}_i$ for $i \in [1, 2, 8]$. Shown for three values of $\mathcal{N}_t$

3.3 Dirac-Delta two parameter study

In the previous section we found a Hopf bifurcation when $\mathcal{N}_t$ exceeded the value at which all size classes were present. With auto-07 we are able to trace this Hopf bifurcation in a second free parameter, which is chosen to be δ_0.

If we follow this Hopf bifurcation with decreasing δ_0, we eventually reach the point where $\delta_0 = 0$. This point is a Bogdanov–Takens bifurcation. Because zooplankton mortality vanishes here, either $\tilde{P}_i$ or $\tilde{Z}_i$ must be zero. If $\tilde{P}_i \neq 0$, so $\tilde{Z}_i = 0$, then $\mu_i \frac{\mathcal{N}}{\mathcal{N}+k_i} = \lambda_i$ for every such i. As the zooplankton never dies it can take on any value and the result would be stationary, this means there are endless solutions here. Because zooplankton are not immortal, we forego further analysis of this bifurcation.

If, instead, we increase δ_0, $\tilde{Z}_8$ decreases. This is seen in Figure 3.3a. The figure plots $\tilde{Z}_8$ against $\mathcal{N}_t$, with $\delta_0 = 0$ at the top-left end of the orange curve. We then follow the orange line for increasing δ_0 till the point at 1 is reached. At this point we have that a second complex pair of the eigenvalues have a real part that is 0. That is we have an Hopf-Hopf bifurcation, interesting mathematical behavior occur at these points, but further analysis is forgone, as it also is not interesting for the larger structure. Instead, we follow the other Hopf branch, which is the remaining blue part. This branch eventually

reaches the point where $\tilde{Z}_8 = 0$ indicated by 2. This coincides with the transcritical bifurcation encountered when the system switched from **P** to **Z**. So we are able to make this switch again, and follow the blue branch into the solution with $\tilde{Z}_8 = 0$ and $\tilde{P}_8 \neq 0$. Here we similarly find that for increasing δ_0 that $\tilde{P}_8$ slowly decreases till it hits 0. Again this is the earlier found transcritical bifurcation, and we can switch back to **Z**. This back and forth repeats and can be seen in Figure 3.3b. Here the vertical axis shows δ_0 and the horizontal axis shows $\mathcal{N}_t$. The lines show the location of the Hopf bifurcation, the points 1 and 2 are the same as in Figure 3.3a. From point 2 to 3, $\tilde{P}_8$ decreases; from 3 to 4, $\tilde{Z}_7$ does; from 4 to 5, $\tilde{P}_7$, and so on. It can be seen that this follows a saw tooth pattern switching back and forth. With each tooth one less size class remains stable.

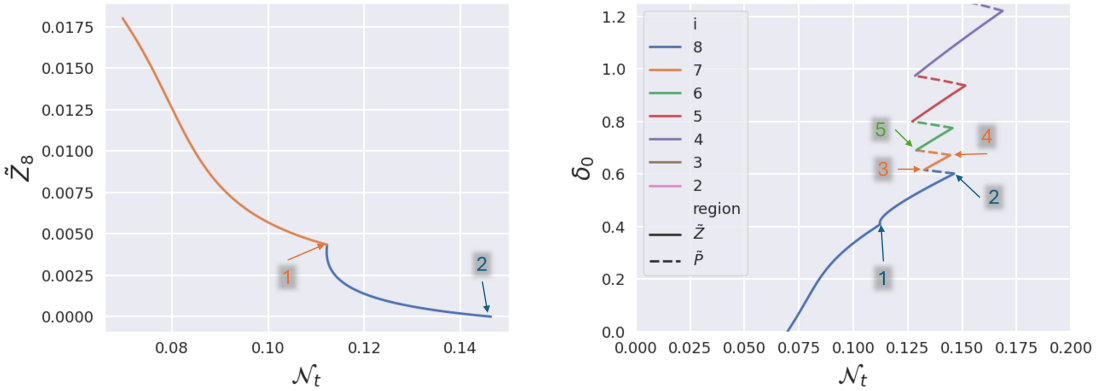

(a) A figure showing the value for $\tilde{Z}_8$ against $\mathcal{N}_t$. Here the line is parameterized by δ_0, where $\delta_0 = 0$ is the left-most point. The orange line is the first encountered Hopf bifurcation, while the blue part is another Hopf bifurcation that crosses over each other at point 1.

(b) A plot showing at which $\mathcal{N}_t$ the Hopf bifurcations occurs for different values of δ_0. Color indicates the number of size classes. Solid lines denote cases where both $\tilde{Z}_i$ and $\tilde{P}_i$ are present, whereas dotted lines indicate that the largest $\tilde{Z}_i$ are absent.

Figure 3.3

Besides the Hopf bifurcation we are also able to trace out the transcritical bifurcations with a freed δ_0. The result is shown in Figure 3.4a. Here we see for different values of δ_0 on the vertical axes the values of $\mathcal{N}_t$ where the transcritical bifurcations happen. The solid lines are the points where we transfer from **Z** to **P**, and the dotted lines the other way. Here we note that for our parameter setting the width of the members **Z** is small in comparison to the members of **P**, so the dotted lines appear under the next solid line. It can be seen that the structure is fan like, where for larger δ_0 the regions of **P** get wider, and thus the total nutrients needed to sustain all size classes increases as well.

Figure 3.4a and the sawtooth of Figure 3.3b can be combined into one picture to get the full overview of where which stationary family member is stable. This can be seen in Figure 3.4b. The diagram summarizes the stationary solution structure in the $(\mathcal{N}_t, \delta_0)$ plane. The lower dotted line is the value of δ_0 used for Figure 2.2. The upper dotted line is at $\delta_0 = 0.96$, and that solution is shown in Figure 3.4c. Its structure is familiar, but the dotted lines now indicate that for $\mathcal{N}_t \approx 0.136$ the family members lose stability.

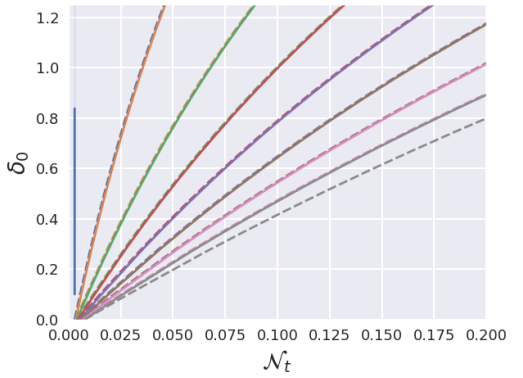

(a) A plot showing at which value of $\mathcal{N}_t$ different transcritical bifurcations happen for a

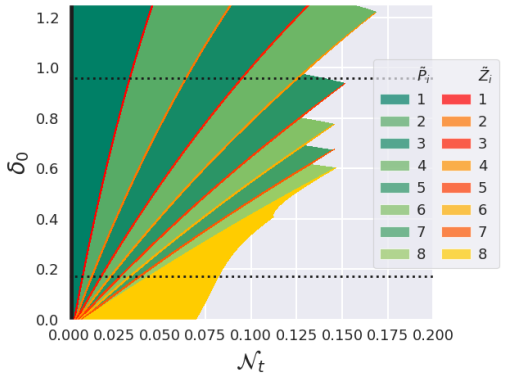

(b) A plot showing regions where different stable solutions are present for a range of δ_0.

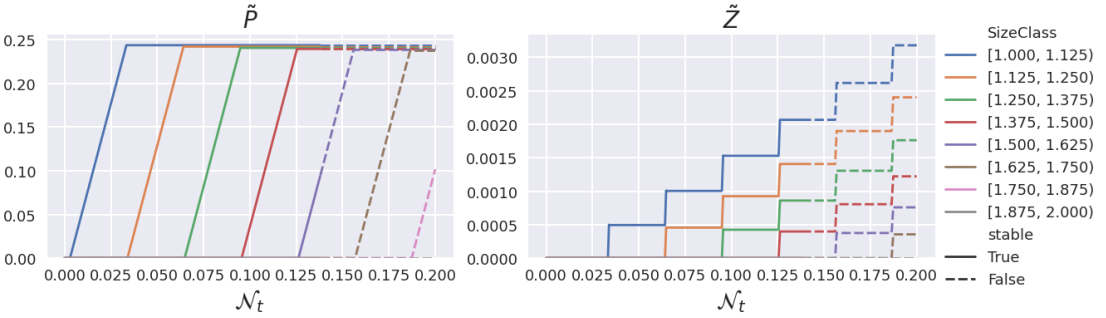

(c) two Figures showing the stable value for different values of $\mathcal{N}_t$. The left showing Phytoplankton size classes and the right Zooplankton size classes

Figure 3.4

The structure of these Hopf bifurcations gave us the key to fully analyze the complete stationary structure. Thus an interesting analysis can be done on how this boundary changes under different choices of Δs_i and n. In Figure 3.5 we see the traced out Hopf bifurcations, for different discretizations. The green line is the same as in Figure 3.3b, with our standard settings. The purple and red lines are with $\Delta s_i = \frac{1}{16}$, the blue with $\frac{1}{4}$. The orange and red lines have 16 size classes instead of 8. The saw-tooth boundary shifts left or right along $\mathcal{N}_t$ when Δs_i is decreased or increased, respectively. Comparing red with green, and blue with orange, shows that finer discretization causes stability to be lost at lower $\mathcal{N}_t$. The exact analytical cause of this shift is unclear; however, with smaller size classes the one-to-one feeding assumption becomes less realistic. This is because the preference of a zooplankton needs to be restricted even further. This might reach the point where the actual biomass within one size class is so small that any zooplankton has almost no chance of finding its exact and only preference.

If we solely increase the number of size classes, by increasing the maximum size. We see that the lines overlap for the size classes that are shared. But for the larger size classes we see that the pattern continues, and it pushes the Hopf bifurcation that was previously encountered first further away. This then means that this first encountered

Hopf bifurcation was due to the lack of a larger size class, and not due to same reason as the saw tooth pattern.

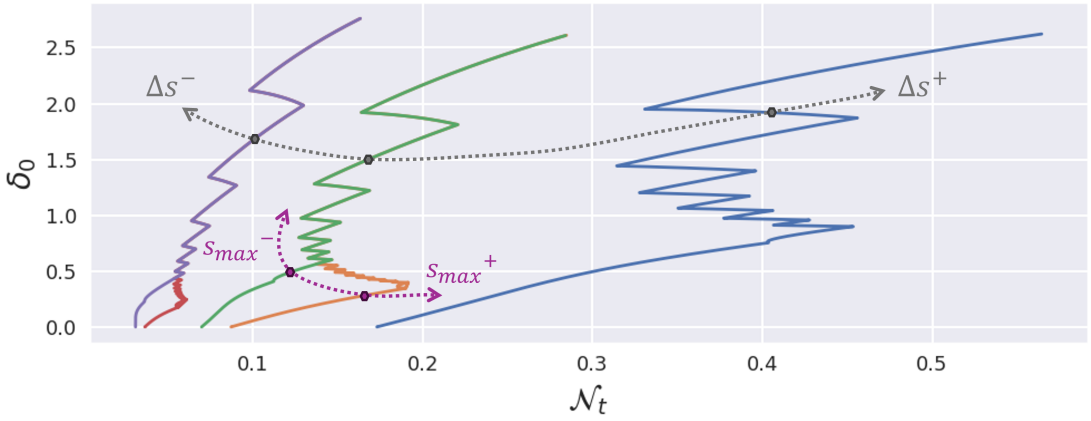

Figure 3.5: Figure showing the Hopf bifurcations that intersect stable regions.

3.4 Dirac delta two parameter limit cycles

In the previous section we saw that the place the Hopf bifurcation was found changed with changing δ_0. To see how δ_0 affects the emergent limit cycle, we first study the branch at $\delta_0 = 0.96$. Three phase diagrams are shown in Figure 3.6 of $\tilde{Z}_i$ against $\tilde{P}_i$, for $i \in \{1,3,5\}$. For each diagram, four different values of $\mathcal{N}_t$ are plotted. The dotted lines represent $\mathcal{P}_i$.

For $i = 1$ and $i = 3$ the high over structure is similar to the one found for $\delta_0 = 0.17$ in section 3.2. That is the structure similar to a classical predator-pray model. More interesting is the bifurcation structure of these cycles. We first have that the blue cycle is just after the Hopf bifurcation, this is still small in amplitude.

The first point of interest is the orange cycle, this is a bifurcation point of the limit cycle. At this bifurcation the stable limit cycle gives way to a branch in which $\tilde{Z}_5$ appears. We can see that this happens as soon as the limit cycle is close to $\mathcal{P}_5$. In the now stable branch we see that with further increasing $\mathcal{N}_t$, the values of $\tilde{Z}_i$ slowly increase as well, which is most obvious for $\tilde{Z}_5$ by the scale. At the green curve we observe a period-doubling bifurcation, whose mechanism remains unresolved. More interestingly we get that these stable limit cycles, just like $\delta_0 = 0.17$, terminate in a torus bifurcation.

The point where for the stationary solution $\tilde{Z}_5$ enters is at $\mathcal{N}_t = 0.15595$. The difference between this and the point where the limit cycles hit a bifurcation point are almost equal, the small difference might be due to the limit cycles being found numerically. This means that the limit cycle itself, and the monodromy matrix might have some small errors, which add up to the difference. More importantly this suggests that some of the structure of the stationary solutions carry over to the limit cycles. To confirm this theory the experiment is repeated for a range of δ_0 and the results are shown in

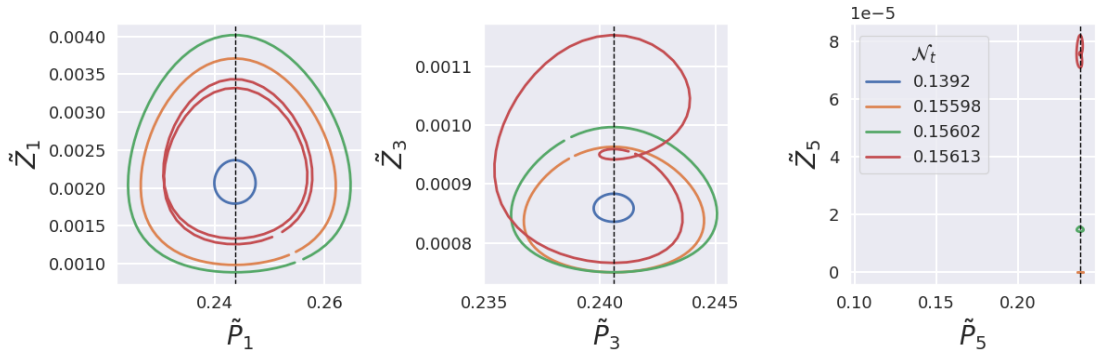

Figure 3.6: Stable limit cycles of $\tilde{P}_i$ and $\tilde{Z}_i$ for $i \in \{1,3,5\}$. Shown for four values of $\mathcal{N}_t$

Figure 3.7. The left panel marks bifurcations at which a new size class appears. The circles denote points where $\tilde{Z}_i$ enters and crosses $\tilde{P}_i$; color indicates i. The blue dotted line gives the Hopf bifurcation found in the previous section, while the dashed lines give the transcritical bifurcations of the stationary system. It is immediately obvious that all these points lay on their stationary counter part, and the differences are negligible. These branches do not persist until all size classes are present; instead, they terminate at a torus bifurcation. The points where this happens are shown in the right pane of Figure 3.7, which is the same as the other picture, but now the points represent where the torus was found. Here one can see that the place where this occurs also follows a similar sawtooth pattern to the Hopf bifurcation of the stationary solutions, but shifted to the right.

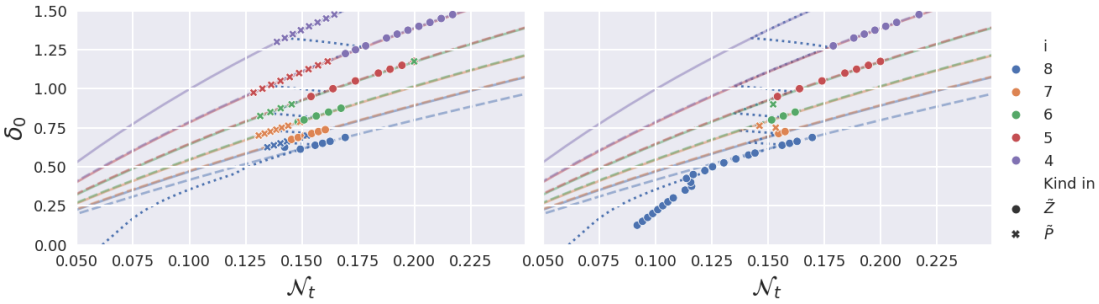

Figure 3.7: two plots showing the location of bifurcation points. The left pane shows the location of the bifurcation points, where another species joins the system. The right pane shows the places where a torus bifurcation was found.

We are unable to continue to follow the stable limit cycle beyond the torus, but the structure found in Figure 3.7 suggests that the number of species present in the non stationary system is closely linked to the number of species in the stationary system. To see if this continues beyond the stable limit cycles we time integrate the system, and after see how many size classes remain after sufficient time to settle has passed. The results are shown in Figure 3.8, here the dots mark spots where the largest size class present was

$\tilde{Z}_i$, while crosses mark points where $\tilde{P}_i$ was the largest. The color of the dot gives which i. The blue dotted line gives the Hopf bifurcations, and the lines give the location of the transcritical bifurcations. Both of these are found in the previous section. It is obvious that beyond the stable limit cycles, the system also closely follows how many species remain. This means that while the stationary points in these regions are unstable, we probably have that these points are saddle points, where in some directions we find that they attract. Consequently, these size classes eventually die out.

There are some subtle differences between the stationary solutions and the results of the numerical time integration. The most notable discrepancies occur near the boundaries where $\tilde{Z}_i$ enters the system. The first difference is seen at the boundary between four and five size classes, from purple to red, where $\tilde{P}_5$ persists. This might be due to the fact that at these points we are close to the boundary found for the stationary solutions, and so we have that for $\tilde{P}_5$ that $\frac{d\tilde{P}}{dt}$ remains close to 0. This results in the fact that it takes a long time for all $\tilde{P}_5$ to leave the system.

A second difference is seen along the boundary from the seventh to eighth size class, where $\tilde{Z}_7$ dies out. This might be due to the fact that the concentrations of $\tilde{Z}_i$ hit such low levels, that numerical accuracy rends them extinct. At these points we get that over a period of 5000 seconds the minimal value of $\tilde{Z}_5 = 3.8 * 10^{-20}$. Which means that we are approaching the floating point limit, and arithmetic with larger numbers will yield large relative errors, which might result in rounding to 0. Once any value is 0 it will forever remain there as there is no way any plankton can start existing without itself. This probably also explains the point where for $\mathcal{N}_t \approx 0.32$ and $\delta_0 \approx 1.3$ we get that $\tilde{P}_7 = 0$.

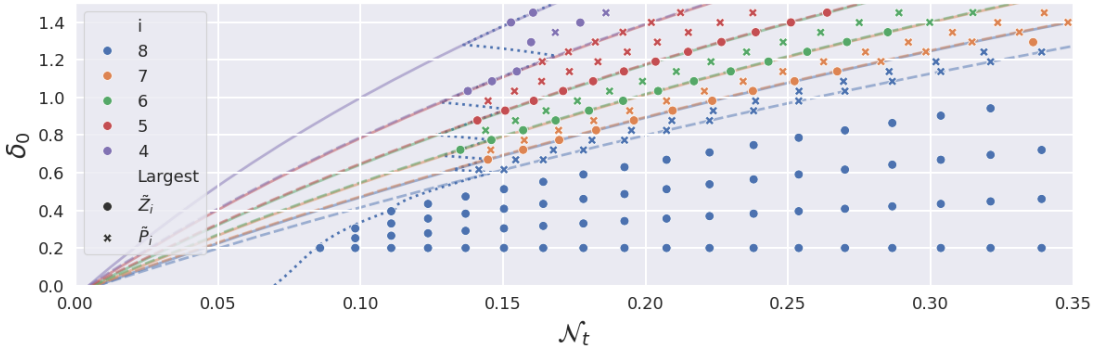

Figure 3.8: A plot showing for a grid of points what species remain after time integrating for 10^5 days. The color gives the number of size classes while circles represent points where $\tilde{Z}_i \neq 0$, and crosses where $\tilde{Z}_i = 0$

We highlight the time series of two points, the first in Figure 3.9, for $\delta_0 = 0.8$ and $\mathcal{N}_t = 0.16$. This point lies just beyond the torus bifurcation, in the region where size classes up to $\tilde{P}_7$ persist. In the figure we can see over a period of 500 for the two kinds of zooplankton the concentration per size class. It can be seen that while the structure shows no exact repeating limit cycle, some structure does remain. First off we see that all concentrations of $\tilde{P}_i$ for $i < 7$ all remain close, while $\tilde{P}_7$ remains halfway. This is inline with the values that we find for the stationary solutions. Furthermore we see that

$\tilde{Z}_{7,8}$ and $\tilde{P}_8$ are not present. For the remaining $\tilde{Z}_i$ we can see that, while not always the case, that we still have that $\tilde{Z}_1 > \tilde{Z}_2 > \cdots > \tilde{Z}_6$. This was also the case for the stationary solutions, and so this structure remains largely in place.

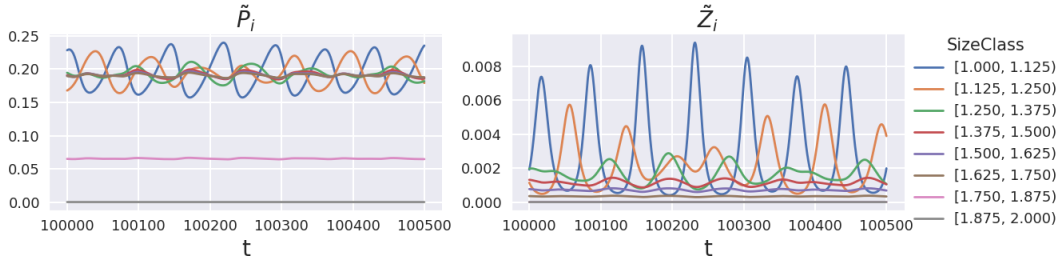

Figure 3.9: two plots showing the time series that remains after 10^5 days. They both show a period of 500 days, for $\delta_0 = 0.8$ and $\mathcal{N}_t = 0.16$. The left and right shows $\tilde{P}_i$ and $\tilde{Z}_i$ respectively. The color gives the size class i.

The second point is shown in Figure 3.10, this is the same plot but for $\delta_0 = 0.33$ and $\mathcal{N}_t = 0.3$. This state lies in the region where all size classes persist but is far from the torus bifurcation It can be clearly seen that at this point the number of present species might correspond to the underlying stationary solution, but all remaining structure is completely gone. At this parameter set the trajectories become almost homoclinic, repeatedly departing from and returning to the saddle at the origin. For the Lotka-Volterra equations this effect is called the "atto-fox problem".

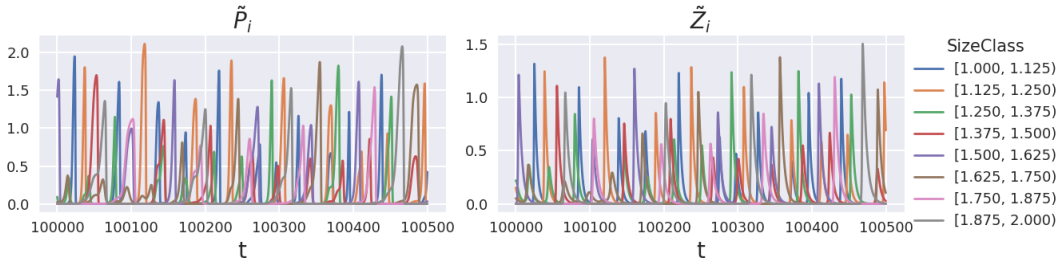

Figure 3.10: two plots showing the time series that remains after 10^5 days. They both show a period of 500 days, for $\delta_0 = 0.33$ and $\mathcal{N}_t = 0.3$. The left and right shows $\tilde{P}_i$ and $\tilde{Z}_i$ respectively. The color gives the size class i.

3.5 Narrow Gaussian kernel

We repeat the analysis done for the Dirac-delta kernel, but for now for system (2.11) with α from (2.12). For this experiment we chose $\Delta s_i = 1/8$ and $\sigma = 1/40$. The found solution structure can be found in Figure 3.11. It can be seen that the structure of these solutions is indeed closely related to the ones found earlier. The phyto- and zooplankton size classes enter the system one after each other. From the smallest till the biggest. When a phytoplankton size class enters the system it increases up to the

point it hits its saturation value and then its zoo- counter part enters. When it enters all already present zooplankton concentrations increase in unison. This continues until all are present, at which point the zooplankton concentrations keep increasing up to where a Hopf bifurcation is met. There are some slight differences, most notably that there is a small overshoot for the phytoplankton when entering the system, but after the next size class enters it drops back down to the same levels found in section 2.5. Because of the overshoot, the exact location where the transcritical bifurcation occurs shifts slightly. This is likely due to the fact that $\tilde{Z}_i$ is able to consume, and thus suppress $\tilde{P}_{i+1}$ from entering the system.

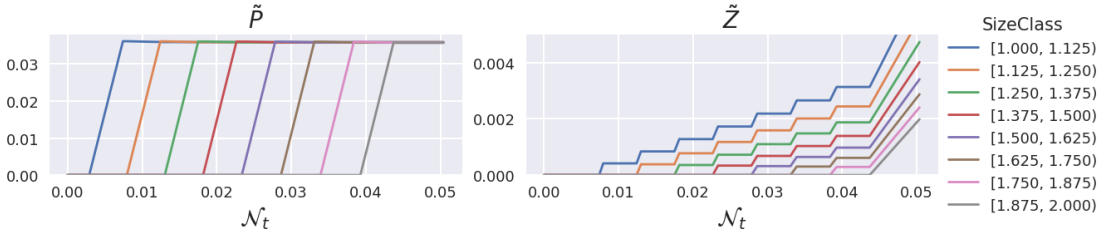

Figure 3.11: two Figures showing the stable value for different values of $\mathcal{N}_t$. The left showing Phytoplankton size classes and the right Zooplankton size classes

3.6 Narrow Gaussian kernel limit cycles

In the previous section we found that eventually the stable stationary solution encounters a Hopf bifurcation. This happens at $\mathcal{N}_t = 7.51 * 10^{-2}$, where it occurred at $\mathcal{N}_t = 8.21 * 10^{-2}$ for the previous system. From this bifurcation we find a stable limit cycle, which is in line with what was found for the Dirac-delta kernel. Some of the found limit cycles are shown in Figure 3.12. Here we can see for four different values of $\mathcal{N}_t$ the stable limit cycle for $\tilde{P}_i$ with $i \in [1, 2, 8]$. The structure closely follows what was found

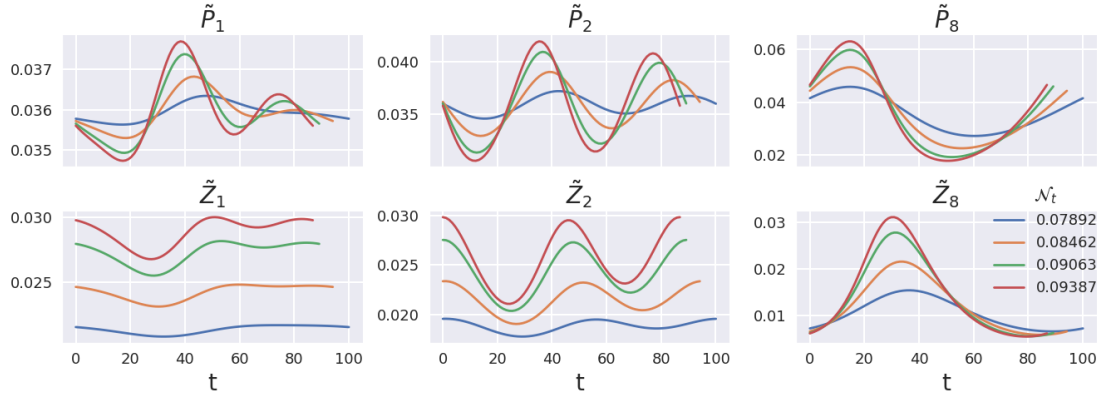

Figure 3.12: Stable limit cycles of $\tilde{P}_i$ and $\tilde{Z}_i$ for $i \in [1, 2, 8]$. Shown for four values of $\mathcal{N}_t$ in section 3.2. Where individual pairs of zoo- and phytoplankton rise and fall just after

each other. These limit cycles also terminate in a torus bifurcation, which now occurs slightly earlier, at $\mathcal{N}_t = 0.09387$ instead of 0.096 in the Dirac-delta case. But we also found that the Hopf bifurcation is a little earlier for this system compared to the simpler system.

3.7 Narrow Gaussian kernel two parameter study

As in section 3.2, increasing $\mathcal{N}_t$ beyond the point where all size classes are present eventually leads to a Hopf bifurcation. This Hopf bifurcation can also be traced with the additional free parameter δ_0. The result is shown in Figure 3.13a, and has the same structure as outlined for Figure 3.3b. To reiterate, we see for a range of δ_0 the value of $\mathcal{N}_t$ at which a Hopf bifurcation is found. Colors indicate the size class i in which the bifurcation occurs; dotted and solid lines distinguish $\tilde{P}_i$ from $\tilde{Z}_i$. It is apparent that this structure is almost identical to the Hopf bifurcation structure for the Dirac delta system in section 3.3. In Figure 3.13b they are shown side by side, and it is clear that besides the structure, also the values are almost identical. The only difference is that the bifurcation is encountered a little further along the respective region.

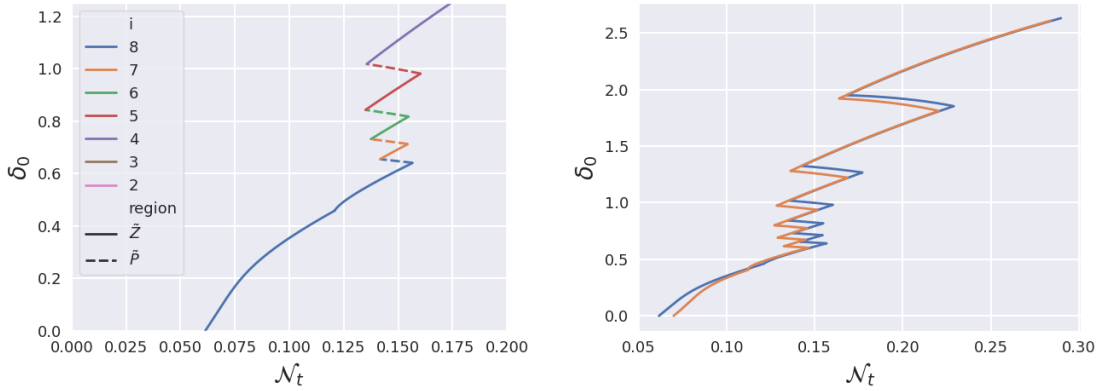

(a) The Hopf bifurcations found for the Gaussian kernel, where the system is stable in the region to the left, and has limit cycle behavior just right to these lines.

(b) The Hopf bifurcation for the Dirac-kernel in orange and the one for the Gaussian kernel with $\sigma = 0.025$ in blue

Figure 3.13

So when choosing α such that that the system is almost the same as the Dirac delta system yields results which are similar. A more thorough conclusion of the implications of this will be given in section 3.10. But before we can fully compare the two system we first have to see how this solution changes under different choices of Δs, and more size classes. In Figure 3.14 this is shown. The red branch corresponds to $\Delta s = 1/16$, the blue to 1/4. The green branch matches Figure 3.13a; the orange branch uses the same Δs but 16 size classes instead of eight. First we note that just like for the Dirac delta system we have that adding larger size classes moves the lower tail part upwards, and thus the first Hopf bifurcation encountered, is again due to the lack of a larger size class.

More notably is that with wider size classes the system moves in the same way as was found in section 3.3. This is explained by the fact that with the same σ, the resulting α is even more like the Dirac delta case. So behavior is expected to be the same. But on the other end we have that refinement of the discretization no longer leads to the shift downward. Instead we see that it stays largely in the same place. Where there was one tooth before, there are two now. The only real difference is the tail part, but again this is due to the lack of larger size classes. Here we have that the refinement made it so our kernel no longer was like the left most example in Figure 2.1, but instead became similar to the second ($\sigma = 0.05$). So this canceled out the movement found earlier. In section 3.9 we will make this statement more concrete by analyzing broader Gaussian kernels.

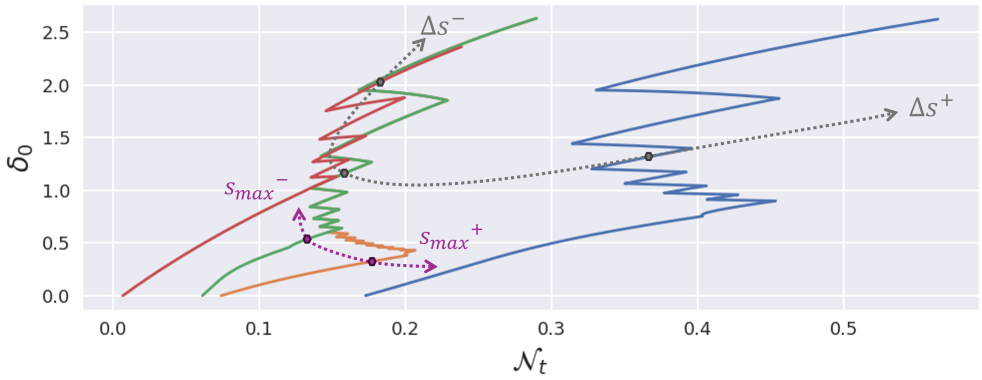

Figure 3.14: a plot showing the Hopf bifurcations for a range of discretization settings. The red, black and green are branches corresponding with Δs being $\frac{1}{16}, \frac{1}{8}$ and $\frac{1}{4}$ respectively. The blue branch has $\Delta s = \frac{1}{8}$, but s_{max} is 3 instead of 2.

3.8 Narrow Gaussian kernel two parameter limit cycles

Just as in section 3.4 we can trace out some stable limit cycles and note where bifurcations do occur. This is shown in Figure 3.15. Here the left pane shows the found branch points, where another Species enters the system. The blue dotted line shows the Hopf bifurcations while the dashed and solid lines show the location of the transcritical bifurcations of the stationary system. We again find that these bifurcation points follow the stationary points closely, and so the structure translates up to the limit cycles.

These stable limit cycles eventually terminate in a torus bifurcation, for which the location is shown in the right pane of Figure 3.15. Here we again see that the underlying saw tooth pattern repeats again but slightly shifted to the right.

Continuing beyond the Torus bifurcation is generally hard, so instead we integrate the system for a long enough time and see how many Species remain. The result is shown in Figure 3.16. Here the circles show points where $\tilde{P}_i \neq 0$, while $\tilde{Z}_i = 0$, while the crosses give points where $\tilde{Z}_i \neq 0$. The color gives which i, the blue dotted line again shows the Hopf bifurcation, while the dashed and solid lines give the location of the

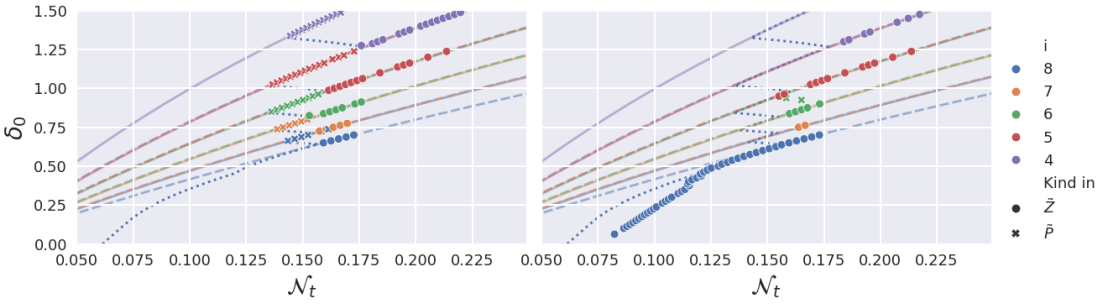

Figure 3.15: two plots showing the location of bifurcation points. The left pane shows the location of the bifurcation points, where another species joins the system. The right pane shows the places where a torus bifurcation was found.

transcritical bifurcations. We once again see that the number of Species present in the stationary solution carries over to the time dependent system. Just like before there are some points where they do not align perfectly, especially for higher values of $\mathcal{N}_t$, the reason for this is similar to what we found earlier, where for these values the numerical errors can become large enough to make $\tilde{Z}_i$ actually go extinct.

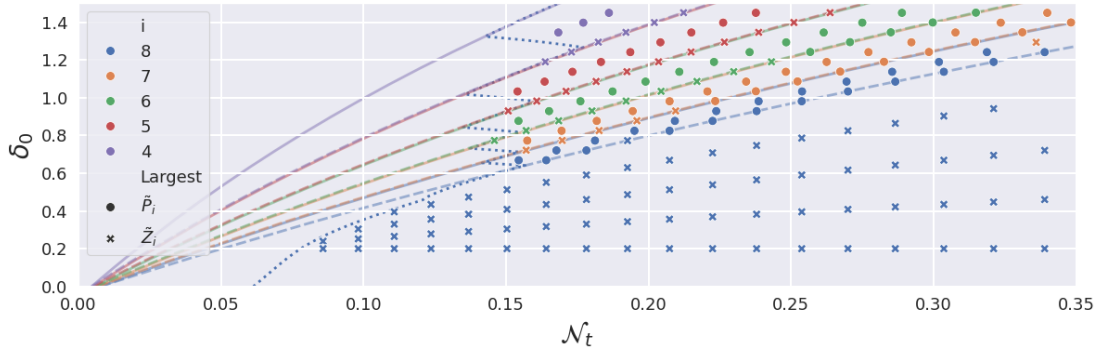

Figure 3.16: A plot showing for a grid of points what Species remain after time integrating for 10^5 days. The color gives the number of size classes while circles represent points where $\tilde{Z}_i \neq 0$, and crosses where $\tilde{Z}_i = 0$

3.9 Gaussian kernel larger deviation

In section 3.7 we ended on the note that further refinement under the same σ led α, away from the form which made the system reduce to the Dirac delta system. This leads to the question what the impact is of the choice of σ versus Δs. For the discretized system we have already seen that if $\Delta s = 5\sigma$, then the the solutions are almost identical. On the other end we expect that for broader feeding kernels that the solutions start to diverge away. We begin with Figure 3.17, which shows the first set of solutions for doubled σ (i.e. $2.5\sigma = \Delta s_i$). The first thing that is obvious is that the overshoot which was present

in the previous section, grows in size. The same mechanism applies: $\tilde{Z}_i$ can consume and therefore suppress $\tilde{P}_{i+1}$. Then we can also note that the gap between $\tilde{Z}_1$ and $\tilde{Z}_2$ is larger. This can be explained by the normalization we chose for α. Because $\tilde{Z}_1$ has a tail into smaller, non-existing size classes we get that both the preference of $\tilde{P}_1$ and $\tilde{P}_2$ increases for it. On the other hand we have that $\tilde{Z}_2$ does not have quite this large of a normalization, and so $\tilde{Z}_1$ hunts more on $\tilde{P}_2$, than $\tilde{Z}_2$ on $\tilde{P}_1$. This becomes more and more apparent for larger σ as can be seen in Figure 2.1.

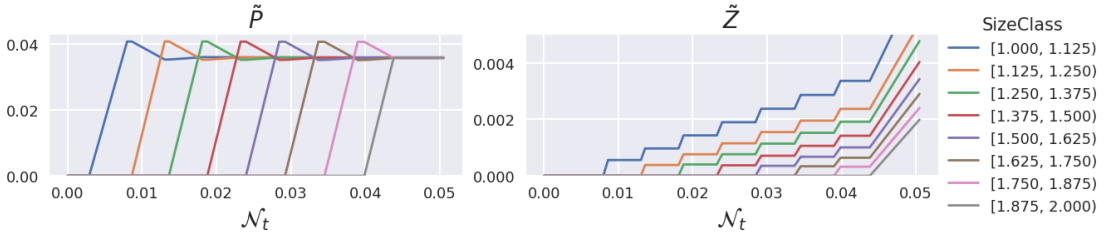

Figure 3.17: two Figures showing the stable value for different values of $\mathcal{N}_t$. Here $2.5\sigma = \Delta s_i = \frac{1}{8}$. The left showing Phytoplankton size classes and the right Zooplankton size classes

We then continue with $1.25\sigma = \Delta s_i$, and the result can be seen in Figure 3.18. It is immediately obvious that the structure that existed before, is no longer present. The overshoots have increased even further in intensity, and only return to the value found for the Dirac delta system above $\mathcal{N}_t \approx 0.035$. To be more precise they drop down the moment the second size class enters the system. This is also the second major difference, the coming of larger size classes is no longer in order. It is largely in order, but the second size class only enters as the sixth. This is again explained by the same reasoning as the previous case. Furthermore we have that the before present ordered stair like structure of $\tilde{Z}_i$ is also almost completely gone. Some plateau-like structure remains, but the values are no longer in descending order. For example the 5th size class, shown in purple, enters the system and goes to a value way higher than the 4th size class, shown in red.

Figure 3.18: two Figures showing the stable value for different values of $\mathcal{N}_t$. Here $1.25\sigma = \Delta s_i = \frac{1}{8}$. The left showing Phytoplankton size classes and the right Zooplankton size classes

The last case studied is $0.625\sigma = \Delta s = \frac{1}{8}$, this system is done for nine size classes instead of the eight done before. It is shown in Figure 3.19. Here we can see that the one by one, from small to big structure is completely lost. Instead after the first size

class the fourth and the fifth appear. The fifth then leaves while the seventh enters. The eighth then enters, which in turn brings back the fifth. Lastly the biggest ninth size class enters, but this forces the eighth out. This structure has no resemblance to the earlier found structure. And so most information gained is lost at this point.

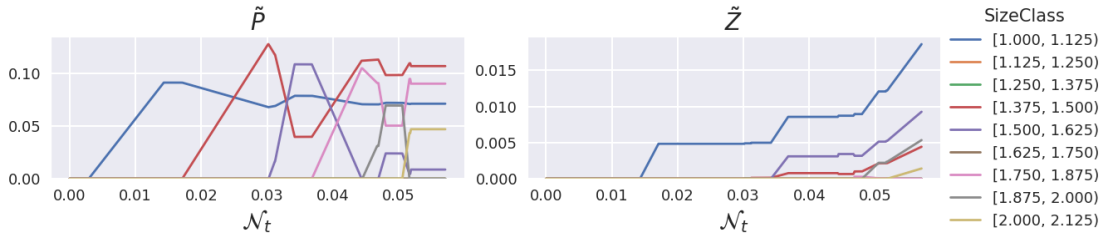

Figure 3.19: two Figures showing the stable value for different values of $\mathcal{N}_t$. Here $0.625\sigma = \Delta s_i = \frac{1}{8}$. The left showing Phytoplankton size classes and the right Zooplankton size classes

For all but the largest standard deviation we can also find the Hopf bifurcation structure. These can be seen in Figure 3.20. The blue, orange and green branch are for $\sigma = \frac{1}{40}, \frac{1}{20}, \frac{1}{10}$ respectively. Increasing σ shifts the structure toward higher $\mathcal{N}_t$, but when σ becomes too large the pattern disintegrates. This break in structure is in line with the break of in structure we found earlier in Figure 3.18. And is due to the second size class being the sixth to join, and thus also the third tooth that we would expect to encounter.

But now we are able to see why the structure did not shift in section 3.7. The decrease in Δs_i made the structure move left, while the relative increase in σ made it move right. These two phenomena cancel each other out and the structure remains in the same place.

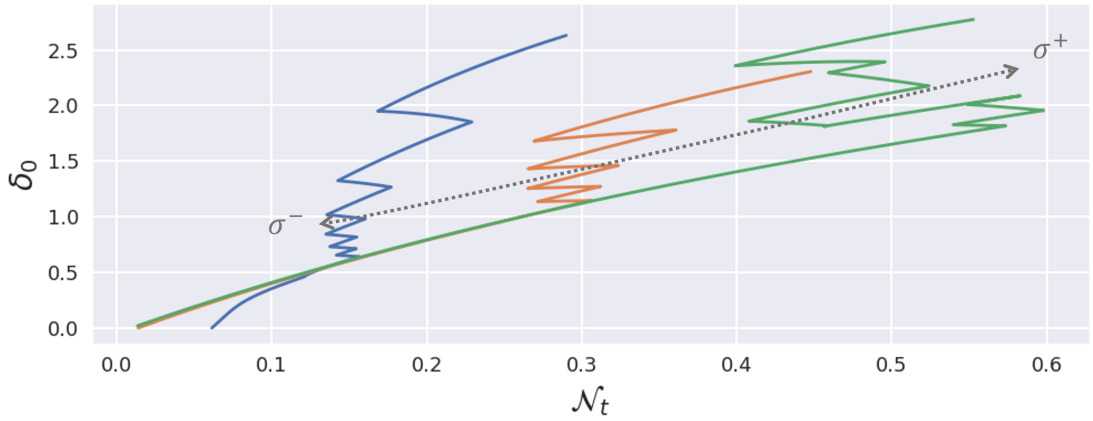

Figure 3.20: A plot showing the Hopf bifurcations. All with $\Delta s = \frac{1}{8}$. The blue, orange and green lines are for $\sigma = \frac{1}{40}, \frac{1}{20}, \frac{1}{10}$ respectively.

3.10 Gaussian from Dirac-Delta

In section 3.1 to section 3.4 we began with an extreme simplification, a Dirac-delta feeding kernel representing perfectly selective predation, which allowed us to get some purely analytical conclusions. This simplification yielded clear insights into the system's behavior, revealing a well-organized bifurcation structure and stability landscape. In particular, the analysis exposed how phytoplankton–zooplankton size classes enter the system sequentially under increasing nutrient supply, each new size class establishing itself in turn until the food web is fully built out. Crucially, we identified the points at which steady-state solutions lose stability via Hopf bifurcations, leading to limit cycles. These analytical and numerical results provided a baseline understanding of the model's dynamics, including explicit conditions for stability and the emergence of complex behaviors, all in a framework that was largely interpretable due to the simplifying feeding assumption.

In section 3.5 till section 3.9 we investigated a model where feeding interactions were generalized using a Gaussian feeding kernel. This extension allowed predators to consume a range of prey sizes around a preferred size, introducing a controlled increase in complexity while preserving a degree of continuity with the original setup. Through numerical bifurcation experiments and simulations, we explored how gradually broadening the feeding kernel, from a near-Dirac narrow Gaussian to increasingly wide distributions, alters the system's dynamics. For small deviations from the delta-kernel, the behavior proved remarkably robust. The characteristic sequence of size-class appearances and disappearances persisted, and the overall stability pattern remained closely aligned with that of the analytically solved case. Only minor quantitative differences were observed under these narrow kernels, such as slight shifts in the nutrient concentration at which bifurcations occurred or small transient overshoots in concentration when new size classes entered. Importantly, however, these differences did not disrupt the structure of the solutions. Thus, within this regime of modest kernel breadth, the complex model retained the essential dynamics and interpretability of the simplified model, indicating that the insights gained from the Dirac-delta analysis are robust to a reasonable range of more realistic feeding behaviors.

As the feeding kernel was widened further, this correspondence began to break down. Once the Gaussian feeding distribution became sufficiently broad, the previously observed orderly pattern of dynamics gave way to new, emergent behavior. The neat stepwise assembly of the plankton community disappeared and the clear bifurcation structure identified in the delta-kernel model became distorted. For example, the distinctive "sawtooth" progression of stable and unstable regions in parameter space was lost as feeding generality increased. In other words, beyond a critical kernel width, the system entered a regime of qualitatively new dynamics that the simplified framework could not anticipate.

This last part might seem as a direct down side of this approach. These two models start diverging with further refinement in discretization, and only with a very specific choice of discretization they actually somewhat align. But the end goal was not giving

a perfect answer to a more complex model, but instead showing how we can gather information relevant for the complex model, at a simpler and tractable level. So the usefulness becomes clear if we turn the steps around. That is we start with some kind of known feeding kernel. Now we do not know anything of what we can expect, but if we discretize $\tilde{P}$ and $\tilde{Z}$ in a way that the resulting α is close enough to the Dirac delta system, then we get a quick, cheap and accessible insight in some structure we might expect.

We have already seen this in Figure 3.13b, but with the reasoning swapped: Suppose we start with a Gaussian kernel of $\sigma = 1/40$ on $\mathcal{S} = [1,2)$. Discretized into eight size classes with $\Delta s_i = 1/8$. This gives us all the insights gathered cheaply with the simplified model, and as shown in Figure 3.13b the stability carries over, and this stays largely the same with further refinement as shown in Figure 3.14. It does break down eventually, and the solutions might become chaotic, but it does give us a hint at how many size classes remain.

A second example is given in Figure 3.21a. Here the we let $\sigma = \frac{1}{20}$, and if we would want to have a similar situation here we need to take $\Delta s_i = \frac{1}{4}$. The orange line shows the result from the Dirac delta system. The blue line is the one we found earlier for $\Delta s_i = \frac{1}{8}$. Here we can see a similar thing, the location of the structures is very close and where the refinement has two tooth's and the simple case has one.

This similarity does break down as shown in Figure 3.21b, for $\sigma = \frac{1}{10}$, in this case $\Delta s = \frac{1}{2}$. The structure for the Dirac system is again shown in orange and this only has two size classes, and its Gaussian counter part in blue. It can be seen that this simplifies too far. We now have that one size class of the Dirac delta system fully encapsulates all the details of the general case, and the found structure are no longer alike.

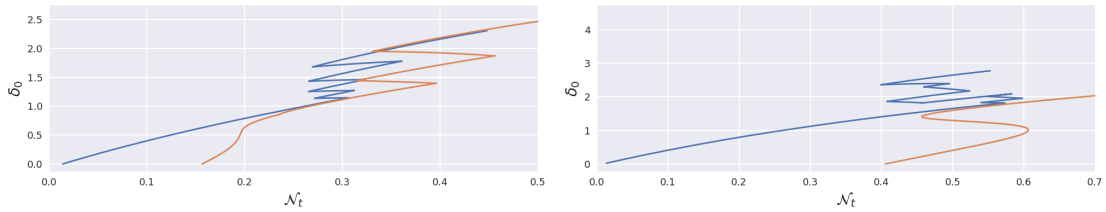

(a) A figure showing in orange the Hopf structure for the Dirac system using $\Delta s = \frac{1}{4}$. In blue the found structure for the general system with $\sigma = \frac{1}{20}$ and $\Delta s_i = \frac{1}{8}$.

(b) A figure showing in orange the Hopf structure for the Dirac system using $\Delta s = \frac{1}{2}$. In blue the found structure for the general system with $\sigma = \frac{1}{10}$ and $\Delta s_i = \frac{1}{8}$.

Figure 3.21

We have also seen that when we limit the Gaussian that the structure of the non stationary solutions for the Dirac delta model also carry over. But at the same time we saw that for the Dirac delta that, within reasonable $\mathcal{N}_t$ and δ_0, that it corresponded with the underlying stationary solution. So while we might not be able to exactly say how a non stationary solution looks like for the Gaussian model. We are able to give a good prediction on how many species, and the approximate values. If we went beyond a reasonable point we lost the ability to say anything about approximate values, but the

amount of species still corresponded well. This means that the cheap analytical solutions found in section 2.5 actually give a lot of information beyond their first appearance.

3.11 Ecological interpretation

In the previous sections we saw that to some extent stability, and solution structures carry over from the simplified model. These solution structures give good insight into the question how many size classes remain in the system. They allow us to make an educated guess in how to discretize a more general applicable setting. This gives us answers to the question how diverse the system is. Some other ecological questions remain unanswered.

The first is question is: how much biomass is in the system? All values that we have shown thus far have been a concentration per size class. This was done as this quantity is not dependent on the choice of discretization, besides that the representative parameter shifts. This allowed us to compare the results side by side, but to answer the question all that remains is multiplying by the respective size class width. Because we look at a range of $\mathcal{N}_t$, we instead opt to look at the quantity $\frac{biomass}{\mathcal{N}_t}$. This quantity can be thought off as the efficiency of the system in utilizing the available resources. In Figure 3.22 we can see for the Dirac delta, and the Gaussian model for $\sigma = \frac{1}{40}$, this efficiency. For the stationary regions this is calculated straight forwardly. For the regions which oscillate we take the average over a period of 500 days. At a first glance these are also fairly similar between the 2 models, which is to be expected as these regions have been behaving similar thus far. To be a little more specific about the implications: For the stationary solutions, the left side of the black line, we can see that the system generally has efficiencies close to 1, except where there is only $\tilde{P}_1$. In this region we have that the biomass goes up from 0, with $\tilde{P}_1 \Delta s_1$, and so the utilization in this area will asymptotically go to 1. Furthermore we see that for smaller δ_0 the efficiency no longer approaches 1 with increasing $\mathcal{N}_t$, instead it goes up to 0.6. So because zooplankton dies at a slower rate it can suppress the phytoplankton from fully utilizing the available resources. This trend continuous into the oscillating region, where for larger amounts of nutrients the systems biomass grows at diminishing rates. In section 3.4 we did find that these cycles almost became homoclinic, where extreme phytoplankton blooms were followed by extreme zooplankton blooms. So this might partly explain the diminishing returns in this area. For larger δ_0 we have that a bloom of phytoplankton, is still followed by a bloom of zooplankton, but because of the higher mortality rate we get that they die off before fully consuming all phytoplankton. This makes it so instead of bouncing radically up and down, the phytoplankton stay within a more constant band.

The second question is how much of the nutrients is turned into biomass. In Figure 3.23 we can see the values for a range of $\mathcal{N}_t$ and δ_0. Again for the same 2 models. we can see that this is almost a mirrored image of the efficiency of the system. For the most part of the plots we can see that the primary production is rather low. For the stationary solutions this is directly linked to the fact that at these points the efficiency is close to 1. This means that $\mathcal{N}$ is rather small, and thus the expression (2.18) is small. For the region where the dynamic system behaves normally we see the same, as the

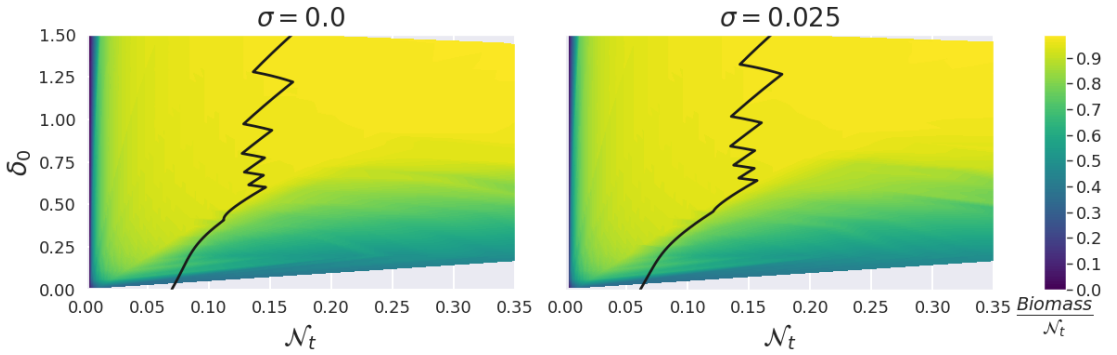

Figure 3.22: The efficiency of the system of 2 models, left the Dirac delta model, right the Gaussian model with $\sigma = 0.025$. The black line denotes the Hopf bifurcations.

resulting system stays close to the values found in the stationary case. During the fast phytoplankton blooms of the system we have high primary production. Then because the zooplankton dies slowly enough to fully, and quickly, consume these blooms, another phytoplankton species get the chance for quick reproduction. This then clearly shows the transition from well behaved to unpredictable with decreasing δ_0.

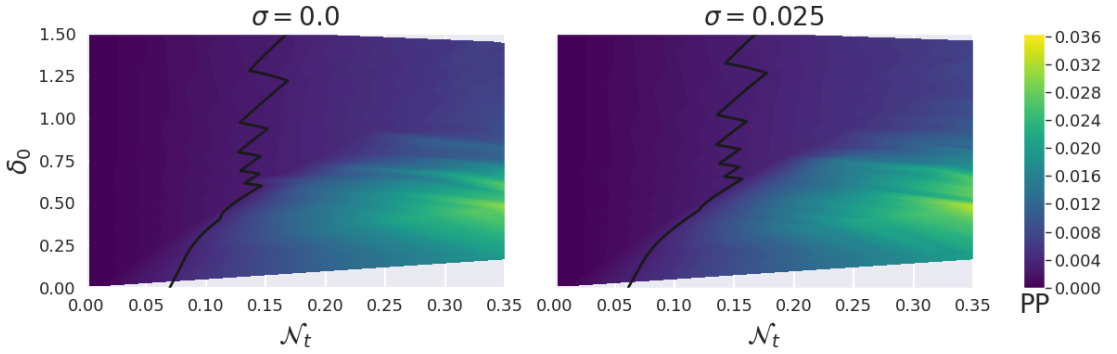

Figure 3.23: The primary production (PP) per day of the system of 2 models, left the Dirac delta model, right the Gaussian model with $\sigma = 0.025$. The black line denotes the Hopf bifurcations.

This might show an apparent weakness in this model. As in this area we have that the immediate availability of nutrients allows the system to behave erratically. Blooming of algae is not unheard off, but quick succession of blooms is not common. Part of this weakness can be alleviated by introducing larger size classes. This is shown in Figure 3.24, where we can see both the primary production and efficiency for a system extended with 8 more size classes. Again the Hopf bifurcations are shown in black. We also added the locations of the transcritical bifurcation where $\tilde{Z}_{16}$ enters the system, these are down as the blue dotted line. It is clear that the areas where the system behaves erratically are mostly below this line. This indicates that some of this behavior is again due to a lack of biodiversity. We can now also better see that in general the

primary production does increase with increased $\mathcal{N}_t$, especially in the non stationary region.

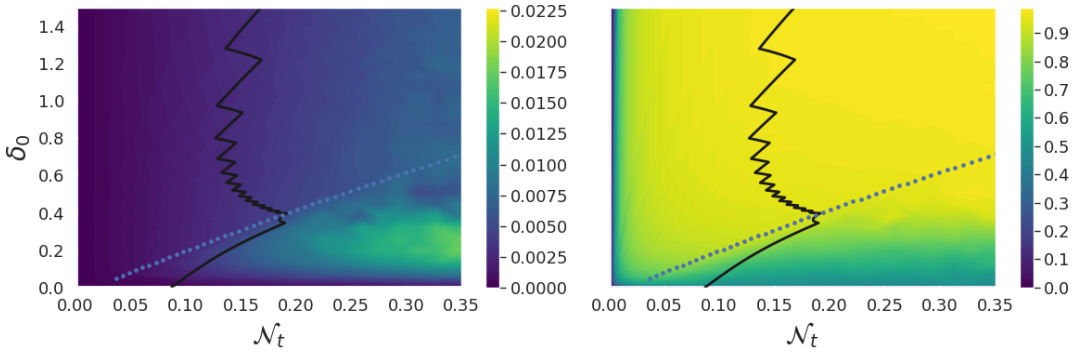

Figure 3.24: Left the average primary production per day, and right the average efficiency. Both for the Dirac delta model, but with $n = 16$, and $s^+ = 3$.

This last part gives us another key insight in giving insights into the more complex models. From the shape of a continuous α we already found directions on how to discretize the system. It remained a question of how many size classes to include to encapsulate all the dynamics. We can now answer this, because we see that in the area where we have (stable) stationary solutions, left and above the green line, the system is rather well behaved. So if we have a $\mathcal{N}_t$ and δ_0, or a range there of, then we have to include enough size classes such that the point lies in a region where the largest $\tilde{Z}_i$ is not yet in the system. This links back all the way to the continuous system, where in section 2.3 we found that with increasing $\mathcal{N}_t$ we had 2 options: Add larger species, or let the zooplankton grow. Now we find that opting for the first choice gives us nice behavior, while choosing for the second makes the system act chaotically. Physically this is understandable, we expect that at some point adding more nutrients increases bio diversity.

3.12 Dirac Delta tool

Motivated by the previous section we have made a tool which is able to generate figures almost like Figure 3.4b. Figure 3.25 shows an example. Note that the output is approximate. The approximation is made using the analytically found values for the bifurcation points as found in section 2.5. Then the stability is calculated for points just inside this region, then the region is drawn for the values that are stable, and interpolated between these points. This means that this is not an exact tool, but it does allow to do a similar analysis as section 3.3 for all input parameters, with minimal effort. The complete tool can be found here (https://github.com/rolfws/npz_model) where the interface is explained in more detail.

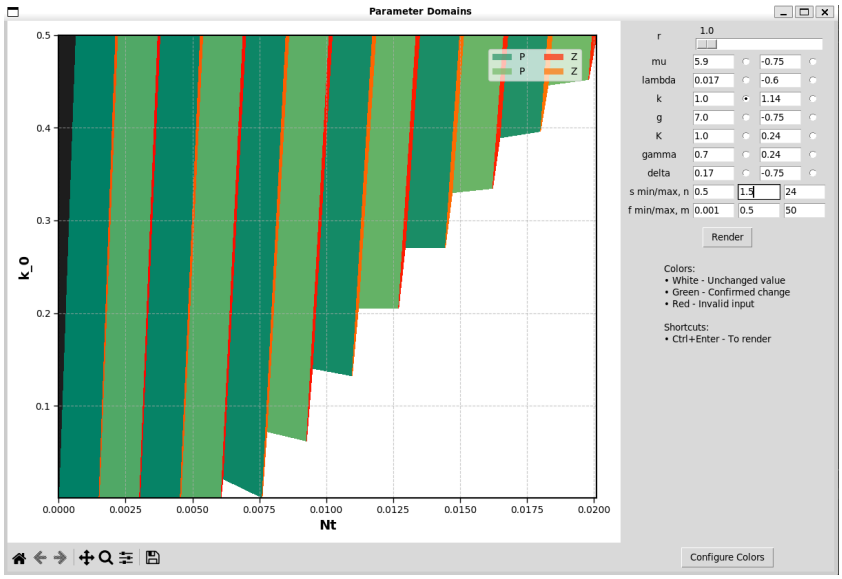

Figure 3.25: Screen shot of the tool, where instead of varying δ_0 we change k_0

Chapter 4

Conclusion

This thesis set out to determine how far the bifurcation structure and stability regimes of a size-structured plankton model with a highly specialized (Dirac-delta) feeding kernel persist under two key generalizations: a more realistic Gaussian feeding kernel and varying numerical discretization. Our results demonstrate that the core dynamical structure of the model is largely robust to these generalizations. In particular, the sequence of bifurcations identified in the Dirac-delta case: A series of transcritical bifurcations leading to non-trivial coexistence equilibria, followed by a Hopf bifurcation giving rise to stable oscillatory dynamics. Remains qualitatively unchanged when the feeding kernel is broadened to a narrow Gaussian form. The bifurcation diagrams for the Dirac and Gaussian models are nearly identical in their overall layout: a phytoplankton-only equilibrium loses stability via transcritical bifurcations at similar critical parameter values, and an interior (phytoplankton–zooplankton) equilibrium subsequently undergoes a Hopf bifurcation to yield predator–prey limit cycles. Likewise, the model's stability regimes (extinction vs. coexistence, steady-state vs. oscillatory dynamics) persist under changes in discretization resolution. Halving or doubling the size-class width Δs (and correspondingly adjusting the number of size classes) did not introduce or eliminate any bifurcations. The same qualitative transitions between regimes occur at essentially the same parameter thresholds across all tested resolutions. In other words, both the feeding kernel generalization and the numerical grid refinement preserve the primary bifurcation architecture of the system. This consistency strongly suggests that the dynamical phenomena uncovered in the simplified Dirac-delta model are not artifacts of an overly special assumption or a particular numerical scheme, but rather are intrinsic features of the plankton–nutrient system.

Despite this overall robustness, certain finer-scale features of the Dirac-delta model's solution structure do not fully carry over under generalization. In the Dirac-delta scenario, the extreme feeding specialization permits a multitude of distinct equilibrium solution branches corresponding to different subsets of plankton size classes persisting. This manifests as a stepped or sequential invasion pattern: as the environment (e.g. total nutrient level or zooplankton mortality rate) changes, each size class can enter or exit the community one at a time, producing a series of transcritical bifurcations at differ-

ent parameter values. Under a broader Gaussian feeding kernel, these multiple solution families are no longer isolated. Feeding generalization couples the size classes, so the previously separate equilibrium branches merge into a single, continuous family of solutions. Consequently, beyond a certain kernel width, the rich multi-branch equilibrium structure observed in the Dirac-delta case collapses into a less diverse configuration: the sequential 'staircase' of transcritical bifurcations disappears, and some of the specialized equilibrium states cease to exist as independent solutions. In practical terms, the model with sufficiently wide feeding kernels exhibits one dominant coexistence equilibrium (and its loss of stability via Hopf) rather than a hierarchy of equilibria appearing in turn.

In summary, the transcritical and Hopf bifurcations, and their associated stability regimes, are robust features of the size-structured plankton model. They persist under the introduction of a Gaussian feeding kernel and remain evident across different discretization resolutions. Aspects that proved not robust to these generalizations are the fine details of the equilibrium structure unique to the Dirac-delta assumption and slight parameter sensitivity at very coarse resolutions. Importantly, the core predator–prey dynamical behavior identified in the idealized model holds in more general settings. This indicates that the insights gained from the simplified Dirac-delta model carry over to more realistic formulations, while clearly delineating which complexities of feeding ecology and numerical representation can alter the system's stability landscape and which do not.

This in turn allows us to turn the flow in opposite direction, where given some general model, we can choose to discretize in a way that was outlined in section 3.10 and section 3.11. This allows us to cheaply evaluate analytical expressions from section 2.5 to give quick insights into where stationary solutions lived, and give some indication into what to expect in non stationary areas.

Chapter 5

Discussion

The bifurcation structure identified here appears robust to moderate changes in feeding kernel shape and discretization granularity. However, several unresolved issues remain that could not be fully addressed in this study. In particular, continuing solution branches beyond torus bifurcations proved difficult, leaving the post-bifurcation dynamics only partially understood. Standard continuation algorithms struggled once a quasi-periodic (torus) solution emerged, highlighting a technical limitation of our analysis. As a result, the long-term behavior of the system in those parameter regimes remains an open question. This challenge invites follow-up approaches, such as direct time integration and phase-space analysis, to characterize the attractors beyond the torus bifurcation points. For example, time-series simulations combined with tools like Poincaré sections or Lyapunov exponent calculations could help discern whether these regimes lead to sustained quasi-periodicity or chaos. Addressing the torus bifurcation issue would thus deepen our understanding of the system's complex oscillatory behavior.

Another limitation is the finite discretization of the size spectrum, which we only explored at a fixed or limited resolution. While the bifurcation patterns were consistent for the tested discretization levels, it remains uncertain how the dynamics converge as one approaches a fully continuous size spectrum. Investigating different discretization schemes or a greater number of size classes would verify the persistence of the observed structures and reveal any subtle numerical artifacts. This presents an opportunity to ask: how fine must the size-class resolution be for the discrete model to reliably reproduce the continuous model's bifurcation behavior? Conversely, what is the impact of extremely coarse discretization on system stability, and where does the simplified representation break down?

To further test the generality of our findings, several natural extensions of the model can be considered. Spatial coupling: Incorporating spatial heterogeneity (for instance, by coupling multiple well-mixed regions or adding diffusion in a spatially extended model) would allow examination of pattern formation and spatial synchrony in the plankton dynamics. A key question is how far one can introduce spatial complexity—even in minimal form—before the bifurcation structure deviates fundamentally from that of the well-mixed (spatially homogeneous) system. Food-web complexity: Increasing the food-

web complexity by adding additional plankton species or trophic levels is a direct way to enhance realism and dimensionality. This extension could reveal richer bifurcation phenomena, but it raises the question of whether the elegant patterns observed in our two-group model persist when the network of interactions is expanded. How far might the simplifying assumptions of our model still predict useful structure as more species and interactions are included, and at what point do new dynamic regimes emerge that are absent in the simpler configuration? Delays and nonlinear responses: Introducing time delays (e.g. gestation or nutrient recycling lags) or more complex functional responses (such as predator satiation beyond the forms considered) would capture important real-world processes. Such additions are expected to influence stability and oscillatory behavior, prompting the question: to what extent can these delayed or highly nonlinear effects be incorporated while retaining a tractable and predictive bifurcation structure akin to the original model?

Each of these extensions represents a research opportunity to probe the limits of our current model's applicability. By exploring spatial dynamics, higher food-web complexity, and more realistic interaction terms, we can assess how robust the identified bifurcation structure remains under increased realism. Ultimately, determining how far the simplified model's insights carry over to more complex scenarios will not only validate those insights but also guide the development of more comprehensive mathematical frameworks for plankton dynamics.

While the analytical structure we found appeared to be stable, no verification was done if it was the only stable branch. To this end more thorough analysis has to be done, by for example finding a suitable Lyapunov function, or by analyzing the Jacobian. An easier tasks would be to check all possible combinations that are outlined in section 2.5, but this group grows exponentially with more size classes. Furthermore we have found solutions for the continuous formulation with a Dirac delta kernel. What we have not done is analyzed spectral properties of this solution, and thus can not say anything about stability, and thus applicability. With further discretization we found that the discretized system became unstable, so it is unexpected that the continuous solution is stable, but still might have time dependent solutions.

Lastly we analyzed how far stationary structure did carry over, but we have not done the same for the time dependent system. We have seen that the structure is similar between the Dirac delta and a narrow Gaussian, but does this also work for a little broader Gaussian? Furthermore we have seen that stationary structure impacts the time dependent structure. But this might also be the case for broader structures, and thus allow us to forgo expensive time integration, but take the results from the stationary bifurcation analysis, and use them to approximate these costly operations. This might be an useful insight if we extend the model up one level further, where now these Gaussian models are the simplified case.

Bibliography

Andersen, K., & Visser, A. (2023). From cell size and first principles to structure and function of unicellular plankton communities. *Progress in Oceanography*, *213*, 102995. https://doi.org/https://doi.org/10.1016/j.pocean.2023.102995

Anderson, T. R. (2005). Plankton functional type modelling: Running before we can walk? *Journal of Plankton Research*, *27*(11), 1073–1081. https://doi.org/10.1093/plankt/fbi076

Basu, S., & Mackey, K. R. M. (2018). Phytoplankton as key mediators of the biological carbon pump: Their responses to a changing climate. *Sustainability*, *10*(3). https://doi.org/10.3390/su10030869

Brauer, F., & Castillo-Chavez, C. (2011, September). *Mathematical models in population biology and epidemiology* (2nd ed.). Springer.

Carlotti, F. (2019). Plankton: Population Dynamics Models. In Cochran, J. K. Bokuniewicz, J. H. Yager, & L. Patricia (Eds.), *Encyclopedia of Ocean Sciences, 3rd Edition* (pp. 571–582, Vol. 5). hal. https://doi.org/10.1016/B978-0-12-409548-9.11472-1

Eedara, K. R. (2016, July 13). Auto-07p - not able to see results for more than 6 states. Retrieved October 10, 2024, from https://www.researchgate.net/post/AUTO-07P-Not-able-to-see-results-for-more-than-6-states-in-the-bifurcation-diagram-Problem-is-solved-without-errors-though

Follows, M. J., Dutkiewicz, S., Grant, S., & Chisholm, S. W. (2007). Emergent biogeography of microbial communities in a model ocean. *Science*, *315*(5820), 1843–1846. https://doi.org/10.1126/science.1138544

Hardin, G. (1960). The competitive exclusion principle. *Science*, *131*(3409), 1292–1297. https://doi.org/10.1126/science.131.3409.1292

Holling, C. S. (1959). The components of predation as revealed by a study of small-mammal predation of the european pine sawfly. *The Canadian Entomologist*, *91*(5), 293–320. https://doi.org/10.4039/Ent91293-5

Huisman, J., & Weissing, F. J. (1999). Biodiversity of plankton by species oscillations and chaos. *Nature*, *402*(6760), 407–410. https://doi.org/10.1038/46540

Hutchinson, G. E. (1961). The paradox of the plankton. *The American Naturalist*, *95*(882), 137–145.

Kolmogorov, A. (1936). Sulla teoria di volterra della lotta per lesistenza. *Gi. Inst. Ital. Attuari*, *7*, 74–80.

May, R. M. (1972). Limit cycles in predator-prey communities. *Science*, *177*(4052), 900–902. https://doi.org/10.1126/science.177.4052.900

Oldeman, B., Paffenroth, R., Sandstede, B., Wang, X., & Zhang, C. (2007). *Auto-07p: Continuation and bifurcation software for ordinary differential equations* (tech. rep.). Concordia University. Concordia University.

Poulin, F. J., & Franks, P. J. S. (2010). Size-structured planktonic ecosystems: Constraints, controls and assembly instructions. *Journal of Plankton Research*, *32*(8), 1121–1130. https://doi.org/10.1093/plankt/fbp145

Seydel, R. (2010). *Practical bifurcation and stability analysis*. Springer New York. https://doi.org/10.1007/978-1-4419-1740-9

Sigmund, K. (2007). Kolmogorov and population dynamics. In É. Charpentier, A. Lesne, & N. K. Nikolski (Eds.), *Kolmogorov's heritage in mathematics* (pp. 177–186). Springer Berlin Heidelberg. https://doi.org/10.1007/978-3-540-36351-4_9

Steele, J. H., & Henderson, E. W. (1992). The role of predation in plankton models. *Journal of Plankton Research*, *14*(1), 157–172. https://doi.org/10.1093/plankt/14.1.157

Strogatz, S. H. (2000). *Nonlinear dynamics and chaos: With applications to physics, biology, chemistry and engineering*. Westview Press.

Ward, B. A., Dutkiewicz, S., Jahn, O., & Follows, M. J. (2012). A size-structured food-web model for the global ocean. *Limnology and Oceanography*, *57*(6), 1877–1891. https://doi.org/https://doi.org/10.4319/lo.2012.57.6.1877

Appendix A

Steele Stationary solutions

We consider the system as given by Steele (Steele & Henderson, 1992):

$$\begin{aligned}
\frac{dP}{dt} &= \frac{N}{N+k}\beta P(1-\frac{P}{\gamma}) - Z\lambda\frac{P^n}{P^n+\mu} \\
\frac{dZ}{dt} &= \alpha\lambda\frac{P^n}{P^n+\mu}Z - \delta Z^m \\
\frac{dN}{dt} &= p\,(N_0 - N) - \frac{N}{N+k}\beta P(1-\frac{P}{\gamma}) + (1-\alpha)\lambda\frac{P^n}{P^n+\mu}Z
\end{aligned} \tag{A.1}$$

If we consider the case where there is an abundance of nutrients, (or k=0). Then the stationary solutions can be found analytically for $m = 1$. We get that $P^n = \frac{\mu\delta}{\alpha\lambda-\delta}$, and then that $Z = \frac{\alpha\beta}{\delta}P(1-\frac{P}{\gamma})$. For $m > 1$ we can find the expression $Z = \left(\frac{\alpha\lambda}{\delta}\frac{P^n}{P^n+\mu}\right)^{\frac{1}{m-1}}$, which then gives that P is the solution to: $\beta(1-\frac{P}{\gamma}) - Z\frac{P^{n-1}}{P^n+\mu} = 0$ For $m = 2$ we get a solvable equation, but for $m > 2$ it is easier to resort to root finding methods. The costs of this are small because the derivative is available analytically.

We now show the general structure for $m, n \in \{1, 2\}$. Where we change δ, but keep the other parameters fixed at $\gamma = 10$, $\lambda = \alpha = \mu = \beta = 1$, $p = 0.3$ and $k = 0.5$. There is some continuous path from the solution found for $k = 0$, to $k = 0.5$, so it is expected that some structure carries over. First we let $m = n = 1$. As seen in figure A.1. It shows that this stationary solution is only stable for high values of δ. There is a singularity of the solution at $\delta = 1$, in which $P \to \infty$. It can also been seen in figure A.2 that for lower values of δ a somewhat periodic solution emerges, but for larger values of δ the solution converges to an equilibrium. Note that there is not a 1 to 1 comparison between the nutrient rich and sparse system. But the switch between stable and unstable remains in the same high/low structure.

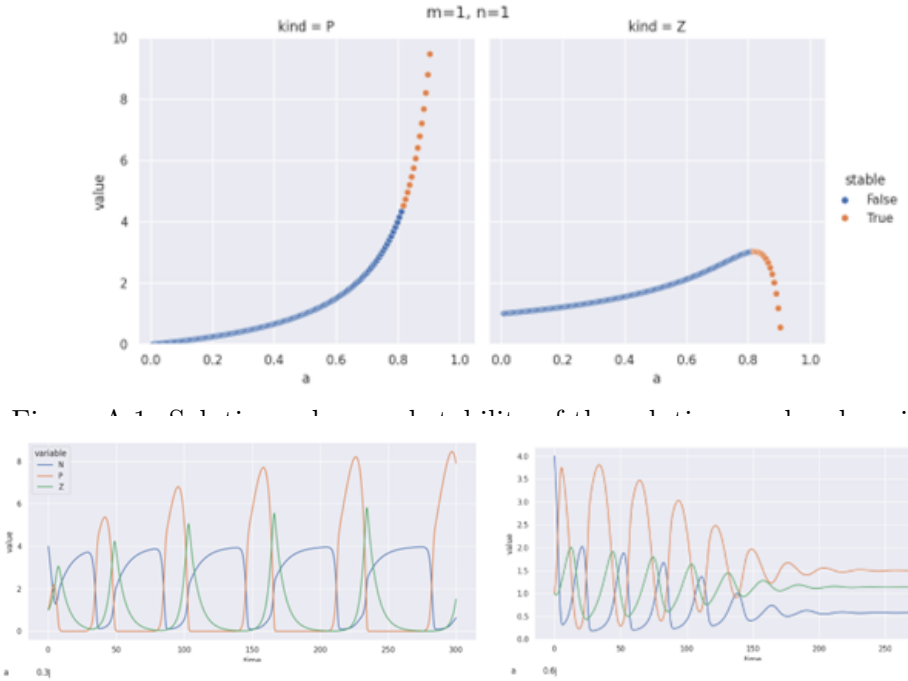

Figure A.2: Time integrated the system with nutrient dependency. On the left if $\delta = 0.3$ and on the right if $\delta = 0.6$

For $m = 1, n = 2$ we get that the solution also has a stable portion at lower values of δ as can be seen in A.3. The stable domain, which started at $\delta \sim 0.8$ for $n = 1$. Now only starts at $\delta \sim 0.95$. This is also found in the nutrient limited system, where the time integration only goes to equilibrium for values of δ close to one. While below 0.95 the cyclic behavior remains. We can also see that the lower stable region carries over.

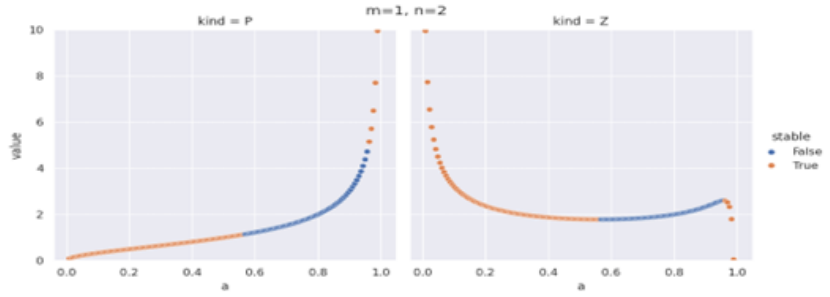

Figure A.3: Solution values and stability of the solutions under changing δ for $m = 1, n = 2$

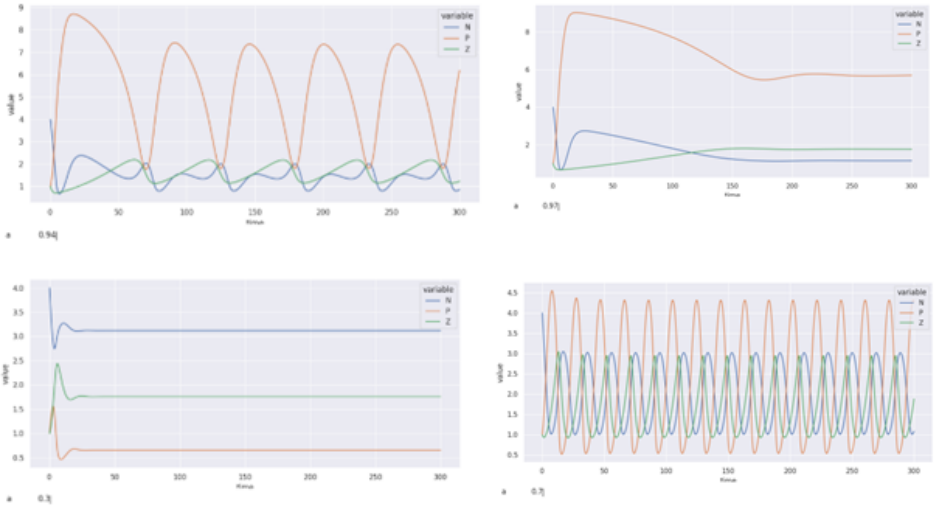

Figure A.4: Time integrated the system with nutrient dependency. From the left top in clockwise order we have $\delta = 0.94$, $\delta = 0.97$, $\delta = 0.3$, $\delta = 0.7$

For $m = 2, n = 1$ the structure does change drastically. Now a fold is introduced as can be seen in figure A.5. The left side of this fold is now unstable while the right is stable from $\delta \sim 0.3$, which is way lower than the value for $m = 1$. The left unstable, right stable structure does remain. This also caries over to the larger system, where cyclic behavior is found for $\delta < 0.3$. And convergence to an equilibrium for larger values. This can be seen in figure A.6.

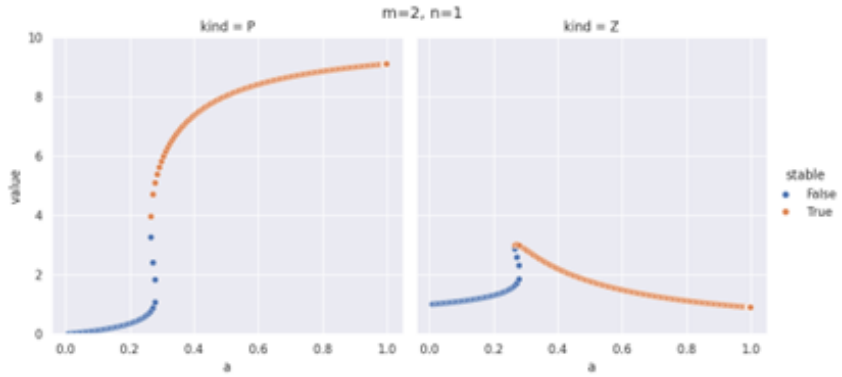

Figure A.5: Solution values and stability of the solutions under changing δ for $m = 2, n = 1$

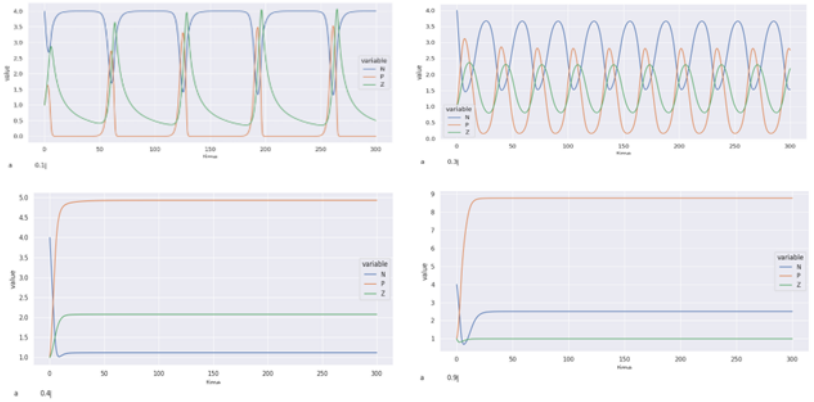

Figure A.6: Time integrated the system with nutrient dependency. From the left top in clockwise order we have $\delta = 0.1$, $\delta = 0.3$, $\delta = 0.4$, $\delta = 0.9$

Now lastly we have $m = n = 2$, the fold remains, but now just like $m = 1, n = 2$ we have that there is a stable region on the left as well. This can be seen in figure A.7. This behavior does carry over to the full system, where each time integration converges to some equilibrium. This is shown for two values of δ in figure A.8.

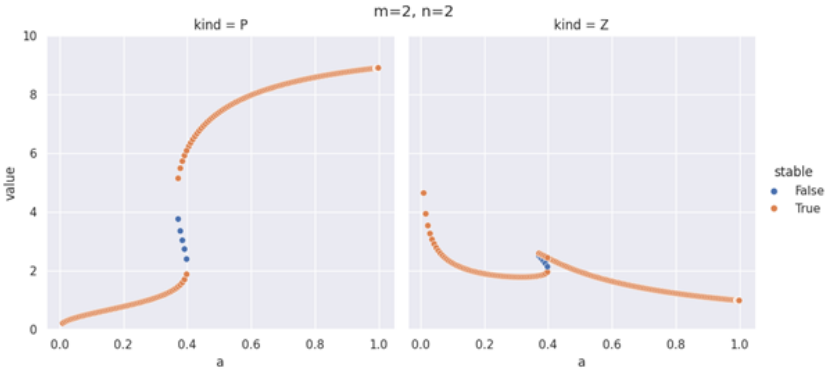

Figure A.7: $m = n = 2$

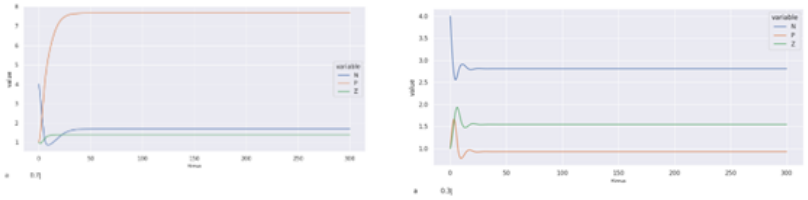

Figure A.8: Time integrated system with nutrient dependency. Left for $\delta = 0.7$ and right for $\delta = 0.3$

This first analysis shows that some behavior found in a simpler model caries over to a fuller model. Furthermore, we can also see how the structure and stability have many similarities between formulations. Further analysis can be done on where between $m = 1$ and $m = 2$ the fold emerges, as there is some homotopy between these 2 solution lines.

A.1 Auto Files and Constants

A.2 Function files (x.c files)

The first function file is for the dirac-delta formulation 2.11:

```
#include "auto_f2c.h"
#include "math.h"
double *var_mu, *var_ld, *var_k, *var_g, *var_K, *var_ga, *var_dt, *
    var_ds, *var_sizes;
double r = 1.0; /*size ratio*/
int set = 0;    /*Variables set on off.*/

/*This function sets the variables for the model using ndim as the number
     of species (#P + #Z)*/
void set_vars(int ndim)
{
  if (!set)
  {
    // start and stop size
    double start = 1.0;
    double stop = 2.0;
```

```
15      // #P/#Z
16      integer hf = ndim / 2;
17      double ds_s = (stop - start) / hf;
18      double size;
19      size_t msize = sizeof(double) * hf;
20      /*
21        For each variable we create a variable size array and fill using
      our scaling.ds_s
22
23        This will leak, but itgets destroyed with the program.
24      */
25      var_mu = (double *)malloc(msize);
26      var_ld = (double *)malloc(msize);
27      var_k = (double *)malloc(msize);
28      var_g = (double *)malloc(msize);
29      var_K = (double *)malloc(msize);
30      var_ga = (double *)malloc(msize);
31      var_dt = (double *)malloc(msize);
32      var_ds = (double *)malloc(msize);
33      var_sizes = (double *)malloc(msize);
34      if (
35          var_mu == NULL || var_ld == NULL || var_k == NULL || var_g ==
      NULL || var_K == NULL || var_ga == NULL || var_dt == NULL || var_ds ==
       NULL || var_sizes == NULL)
36      {
37        printf("allocation failed\n");
38        exit(0);
39      }
40      for (int n = 0; n < hf; n++)
41      {
42        size = start + ds_s * n;
43        var_mu[n] = 5.9 * pow(size, -0.75);
44        var_ld[n] = 0.017 * pow(size, -0.6);
45        var_k[n] = 1.0 * pow(size, 1.14);
46        var_g[n] = 7.0 * pow(size * r, -0.75);
47        var_K[n] = 1.0 * pow(size * r, 0.24);
48        var_ga[n] = 0.7 * pow(size * r, 0.24);
49        var_sizes[n] = size;
50        // var_dt[n] = 0.61 * pow(size * r, -0.75); // 0.61 for 8sys
51        var_ds[n] = ds_s;
52      }
53      set = 1;
54    }
55  }
56
57  int func(integer ndim, const double *u, const integer *icp,
58           const double *par, integer ijac, double *f, double *dfdu, double
       *dfdp)
59  {
60    set_vars(ndim); // Will only set once.
61    double Nt;
62    integer i;
63    integer hf = ndim / 2;
```

```
64    Nt = par[0];
65    // Calculate the biomass to find N
66    double biomass = 0;
67    for (i = 0; i < hf; i++)
68    {
69      var_dt[i] = par[1] * pow(var_sizes[i] * r, -0.75);
70      biomass += u[i] * var_ds[i];
71      biomass += u[i + hf] * var_ds[i] * r;
72    }
73    double N = Nt - biomass;
74    // Evaluate the system
75    for (i = 0; i < hf; i++)
76    {
77      // dP/dt
78      f[i] = u[i] * (var_mu[i] * N / (N + var_k[i]) - var_ld[i] - var_g[i]
        * u[i + hf] / (u[i] + var_K[i]));
79      // dZ/dt
80      f[i + hf] = u[i + hf] * (var_ga[i] * var_g[i] * u[i] / (u[i] + var_K[
        i]) - var_dt[i]);
81    };
82    return 0;
83  }
84  /*
85    Start point fn
86  */
87  int stpnt(integer ndim, double t, double *u, double *par)
88  {
89    par[0] = 0.0;
90    par[1] = 0.17;
91    for (integer i = 0; i < ndim; i++)
92    {
93      u[i] = 0.0;
94    }
95    return 0;
96  }
97  /*
98    Custom output functions
99  */
100 int pvls(integer ndim, const double *u, double *par)
101 {
102   return 0;
103 }
104
105 /*
106   Boundary conditions
107 */
108 int bcnd(integer ndim, const doublereal *par, const integer *icp, integer
        nbc,
109          const doublereal *u0, const doublereal *u1, integer ijac,
110          doublereal *f, doublereal *dbc) { return 0; }
111
112 /*
113   Initial conditions
```

```
114 */
115 int icnd(integer ndim, const doublereal *par, const integer *icp, integer
        nint,
116           const doublereal *u, const doublereal *uold, const doublereal *
        udot,
117           const doublereal *upold, integer ijac,
118           doublereal *fi, doublereal *dint) { return 0; }
119
120 /*
121   Objective function ??
122 */
123 int fopt(integer ndim, const doublereal *u, const integer *icp,
124           const doublereal *par, integer ijac,
125           doublereal *fs, doublereal *dfdu, doublereal *dfdp) { return 0;
        }
```

For the general function we have the following:

```
1  #include "auto_f2c.h"
2  #include "math.h"
3  double *var_mu, *var_ld, *var_k, *var_g, *var_K, *var_ga, *var_dt, *
       var_ds, *var_sizes, *kernel;
4  double r = 1.0; /*size ratio*/
5  int set = 0;    /*Variables set on off.*/
6
7  /*
8    Reads the kernel array from a binary file in row major order.
9    So the second element is the first row and the second column.
10 */
11 void read_array(int n, double *out)
12 {
13   FILE *ptr;
14   size_t s;
15   ptr = fopen("kernel_array.bin", "rb");
16   if (ptr == NULL)
17   {
18     printf("kernel file not found");
19     exit(0);
20   }
21   for (int i = 0; i < n; i++)
22   {
23     s = fread((void *)(&out[i]), sizeof(*out), 1, ptr);
24     if (s != 1) {
25       printf("failed kernel read\n");
26       exit(0);
27     }
28   }
29 }
30
31 void set_vars(int ndim)
32 {
33   if (!set)
34   {
35     double start = 1.0;
```

```
36      double stop = 2.0;
37      integer hf = ndim / 2;
38      double ds_s = (stop - start) / hf;
39      double size;
40      size_t msize = sizeof(double) * hf;
41      /* This will leak, but I do not really care, get destroyed with the
        program*/
42      var_mu = malloc(msize);
43      var_ld = malloc(msize);
44      var_k = malloc(msize);
45      var_g = malloc(msize);
46      var_K = malloc(msize);
47      var_ga = malloc(msize);
48      var_dt = malloc(msize);
49      var_ds = malloc(msize);
50      var_sizes = malloc(msize);
51      kernel = malloc(msize * hf);
52      if (
53          var_mu == NULL || var_ld == NULL || var_k == NULL || var_g ==
        NULL || var_K == NULL || var_ga == NULL || var_dt == NULL || var_ds ==
         NULL || var_sizes == NULL || kernel == NULL)
54      {
55        printf("allocation failed\n");
56        exit(0);
57      }
58
59      read_array(hf * hf, kernel);
60      for (int n = 0; n < hf; n++)
61      {
62        size = start + ds_s * n;
63        var_mu[n] = 5.9 * pow(size, -0.75);
64        var_ld[n] = 0.017 * pow(size, -0.6);
65        var_k[n] = 1.0 * pow(size, 1.14);
66        var_g[n] = 7.0 * pow(size * r, -0.75);
67        var_K[n] = 1.0 * pow(size * r, 0.24);
68        var_ga[n] = 0.7 * pow(size * r, 0.24);
69        var_sizes[n] = size;
70        // var_dt[n] = 0.61 * pow(size * r, -0.75); // 0.61 for 8sys
71        var_ds[n] = ds_s;
72      }
73      set = 1;
74    }
75  }
76
77  int func(integer ndim, const double *u, const integer *icp,
78           const double *par, integer ijac, double *f, double *dfdu, double
         *dfdp)
79  {
80    set_vars(ndim);
81    double Nt, peaten;
82    integer i, j;
83    integer hf = ndim / 2;
84    Nt = par[0];
```

```
85    double biomass = 0, F[hf];
86    for (i = 0; i < hf; i++)
87    {
88      var_dt[i] = par[1] * pow(var_sizes[i] * r, -0.75);
89      biomass += u[i] * var_ds[i];
90      biomass += u[i + hf] * var_ds[i] * r;
91      F[i] = 0.0;
92      for (j = 0; j < hf; j++)
93      {
94        F[i] += kernel[i * hf + j] * u[j] * var_ds[j];
95      }
96    }
97    double N = Nt - biomass;
98    for (i = 0; i < hf; i++)
99    {
100     peaten = 0.0;
101     for (j = 0; j < hf; j++)
102     {
103       peaten += kernel[j * hf + i] * var_g[j] * u[hf + j] / (F[j] + var_K
      [j]) * var_ds[j] * r;
104     }
105     f[i] = u[i] * (var_mu[i] * N / (N + var_k[i]) - var_ld[i] - peaten);
106
107     f[i + hf] = u[i + hf] * (var_ga[i] * var_g[i] * F[i] / (F[i] + var_K[
      i]) - var_dt[i]);
108   };
109   return 0;
110 }
111 /*
112   Start point fn
113 */
114 int stpnt(integer ndim, double t, double *u, double *par)
115 {
116   par[0] = 0.0;
117   par[1] = 0.17;
118   for (integer i = 0; i < ndim; i++)
119   {
120     u[i] = 0.0;
121   }
122   return 0;
123 }
124 /*
125   ??
126 */
127 int pvls(integer ndim, const double *u, double *par)
128 {
129   return 0;
130 }
131
132 /*
133   Boundary conditions
134 */
135 int bcnd(integer ndim, const doublereal *par, const integer *icp, integer
```

```
    nbc,
136         const doublereal *u0, const doublereal *u1, integer ijac,
137         doublereal *f, doublereal *dbc) { return 0; }
138
139 /*
140   Initial conditions
141 */
142 int icnd(integer ndim, const doublereal *par, const integer *icp, integer
    nint,
143         const doublereal *u, const doublereal *uold, const doublereal *
    udot,
144         const doublereal *upold, integer ijac,
145         doublereal *fi, doublereal *dint) { return 0; }
146
147 /*
148   Objective function ??
149 */
150 int fopt(integer ndim, const doublereal *u, const integer *icp,
151         const doublereal *par, integer ijac,
152         doublereal *fs, doublereal *dfdu, doublereal *dfdp) { return 0;
    }
```

The only real difference between the two is the addition for a general matrix α. This matrix is read in the read_array function. This is read from a binary file, consisting of n^2 float64 values. Where the array is stored in row major. To create this array the following numpy script is used:

```
1  import sys
2  import numpy as np
3  from scipy.stats import norm
4
5
6  def main():
7      '''
8          Outputs the gaussian feeding kernel to a file.
9
10         data is ordered row wise, where each row is the sampled kernel
    for Zooplankton class i.
11         This assumes linear size classes. Where the kernel is sampled
    halfway.
12     '''
13     if len(sys.argv) < 5:
14         raise ValueError("Not enough arguments")
15     smin = float(sys.argv[1])
16     smax = float(sys.argv[2])
17     n = int(sys.argv[3])
18     sigma = float(sys.argv[4])
19
20     ds = (smax - smin) / n
21     Psizes = np.linspace(smin, smax, n, endpoint=False) + ds/2
22
23     b = (norm.cdf(Psizes + ds/2, loc=Psizes[:, None], scale=sigma) - norm
    .cdf(Psizes - ds/2, loc=Psizes[:, None], scale=sigma)) / ds
```

```
24      normalizer = norm.cdf(smax, loc=Psizes, scale=sigma) - norm.cdf(smin,
        loc=Psizes, scale=sigma)
25      b /= normalizer[:, None]
26      print(b.astype(float).round(1))
27
28      b.tofile('kernel_array.bin')
29
30  if __name__ == "__main__":
31      main()
```

Now this is called using python kern.py (smin) (smax) (n) (σ). For example python kern.py 1.0 2.0 8 0.025. The output of this script has to be put in the same directory as the .c file.

A.3 constants

For a detailed explanation of each constant we refer to the manual of auto. We used the recommended settings together with the following:

Constant	Value
parnames	{1:'Nt', 2:'d'}
ICP	['Nt', 'd']
NDIM	n
DSMIN	10^{-6}-10^{-4}
DS	10 * DSMIN
DSMAX	100 * DSMIN
NPAR	2

The scripts contain references to constant files with the name c.gausX These only differ in DSMIN, where gaus has a DSMIN of 10^{-6}, gaus2 10^{-5}, gaus3 10^{-4} and lastly gaus4 10^{-3}. These were put into files mostly because of ease of use when using the CLI. For the scripts these could also be hard coded if one likes.

Appendix B

Auto scripts

The following scripts are a general skeleton of scripts that *could* work for different parameter, and or parameter values. Most likely some tuning to the step size setting must be done. For more general kernels these scripts might fail all together and a lot of manual work has to be done. For the dirac delta kernel these scripts will most likely work the best. The scripts are given in the order in which they should be run.

The first script is for the first bifurcations:

```
prev_run = run("pf", c="gaus", STOP=["BP1"])
runs = prev_run
while prev_run("BP"):
    if len(runs) % 2 == 1:
        next_run = run(prev_run("BP1"), ISW=-1, c="gaus3", STOP=["BP1"])
    # elif len(runs) in [4]:
    #     next_run = run(prev_run("BP1"), ISW=-1, c="gaus2", STOP=["BP1
    "])
    else:
        switch = run(prev_run("BP1"), ISW=-1, c="gaus3", STOP=["BP1"],
    NMX=2)
        next_run = run(switch()[0], ISW=1, c="gaus", STOP=["BP1"])

    # if next_run("BP"):
    runs += next_run
    prev_run = next_run
    if len(runs) > 36:
        break
plot(runs)
save(runs, "first_bif")
wait()
```

This script now stops after 36 branches. It is recommended to keep an upper bound on the number of branches, as it can be possible to set step sizes for which the same branch is found over and over again, never leaving this loop.

The second script follows the first found hopf bifurcation. This part might be highly problem specific, and for the more general case this almost always needed to be done manually:

```
bch = loadbd("first_bif")
bchex = run(bch()[-1], ISW=1, c="gaus2", NMX=5000, STOP=["HB1"])
switch = run(bchex("HB1"), ISW=-2, c="gaus4", NMX=5, NPR=1)
hb1 = run(switch()[-1], ISW=2, c="gaus3", STOP=["BP1", "ZH1"]) + run(
    switch()[-1], ISW=2, c="gaus3", STOP=["BP1", "ZH1"], DS="-")
hb1 = merge(hb1)
hbnex = run(hb1("ZH1"), ISW=2, NMX=20, NPR=5)
t = run(hbnex()[-1], ISW=1, DS="-", STOP=["HB2"], c="gaus2")
switch = run(t("HB1"), ISW=-2, c="gaus4", NMX=5, NPR=1)
hb2 = run(switch()[-1], ISW=2, c="gaus3", STOP=["BP1", "ZH1"]) + run(
    switch()[-1], ISW=2, c="gaus2", STOP=["BP1", "ZH1"], DS="-")
hb2 = merge(hb2)
plot(hb1+hb2 + t)
save(hb1+hb2, "first_hopf_part")
wait()
```

Then the last script is to follow the saw tooth pattern of hopf bifurcations:

```
runs = loadbd("first_hopf_part")
prev_run = runs[1:]
while prev_run("BP"):
    if len(runs) % 2 == 1:
        next_run = run(prev_run("BP1"), ISW=-2, c="gaus3", STOP=["BP1"],
    NMX=1000, UZSTOP={}, NPR=50)
    else:
        next_run = run(prev_run("BP1"), ISW=-2, c="gaus3", DS="-", STOP=[
    "BP1"], NMX=2000, UZSTOP={}, NPR=50)
    runs += next_run
    prev_run = next_run

plot(runs)
save(runs, "hopf_bifs")
wait()
```